THE JOURNAL OF COMPARATIVE NEUROLOGY 438:353–376 (2001)

Cytology of Human Caudomedial Cingulate, Retrosplenial, and Caudal Parahippocampal Cortices

BRENT A. VOGT,[1,2] LESLIE J. VOGT,[1,2] DANIEL P. PERL,[3] AND PATRICK R. HOF[4]
[1]Cingulum NeuroSciences Institute, Winston-Salem, North Carolina 27101
[2]Department of Physiology and Pharmacology, Wake Forest University School of Medicine, Winston-Salem, NC 27157-1083
[3]Fishberg Research Center for Neurobiology and Departments of Pathology and Psychiatry, Mount Sinai School of Medicine, New York, New York 10029-6574
[4]Kastor Neurobiology of Aging Laboratories and Fishberg Research Center for Neurobiology and Departments of Geriatrics and Adult Development, Mount Sinai School of Medicine, New York, New York 10029-6574

ABSTRACT

Brodmann showed areas 26, 29, 30, 23, and 31 on the human posterior cingulate gyrus without marking sulcal areas. Histologic studies of retrosplenial areas 29 and 30 identify them on the ventral bank of the cingulate gyrus (CGv), whereas standardized atlases show area 30 on the surface of the caudomedial region. This study evaluates all areas on the CGv and caudomedial region with rigorous cytologic criteria in coronal and oblique sections Nissl stained or immunoreacted for neuron-specific nuclear binding protein and nonphosphorylated neurofilament proteins (NFP-ir). Ectosplenial area 26 has a granular layer with few large pyramidal neurons below. Lateral area 29 (29l) has a dense granular layer II-IV and undifferentiated layers V and VI. Medial area 29 (29m) has a layer III of medium and NFP-ir pyramids and a layer IV with some large, NFP-ir pyramidal neurons that distinguish it from areas 29l, 30, and 27. Although area 29m is primarily on the CGv, a terminal branch can extend onto the caudomedial lobule. Area 30 is dysgranular with a variable thickness layer IV that is interrupted by large NFP-ir neurons in layers IIIc and Va. Although area 30 does not appear on the surface of the caudomedial lobule, a terminal branch can form less that 1% of this gyrus. Area 23a is isocortex with a clear layer IV and large, NFP-ir neurons in layers IIIc and Va. Area 23b is similar to area 23a but with a thicker layer IV, more large neurons in layer Va, and a higher density of NFP-ir neurons in layer III. The caudomedial gyral surface is composed of areas 23a and 23b and a caudal extension of area 31. Although posterior area 27 and the parasubiculum are similar to rostral levels, posterior area 36′ differs from rostral area 36. Subregional flat maps show that retrosplenial cortex is on the CGv, most of the surface of caudomedial cortex is areas 23a, 23b, and 31, and the retrosplenial/parahippocampal border is at the ventral edge of the splenium. Thus, Brodmann's map understates the rostral extent of retrosplenial cortex, overstates its caudoventral extent, and abridges the caudomedial extent of area 23. J. Comp. Neurol. 438:353–376, 2001.

Indexing terms: cytoarchitecture; cingulate gyrus; neurofilament proteins; isocortex; dysgranular cortex; flat maps; Brodmann nomenclature

Brodmann (1909) identified the human ectosplenial area 26, retrosplenial areas 29 and 30, posterior cingulate areas 23 and 31, and parahippocampal areas 27 and 36 and mapped them onto the convoluted medial surface. Although this account did not demonstrate the architecture of each area, subsequent histologic studies confirmed the presence of the ectosplenial and retrosplenial areas on the ventral bank of the cingulate gyrus (CGv) (von Economo and Koskinas, 1925; Rose, 1928; Braak, 1979;

Grant sponsor: NIH; Grant number: NINDS NS38485; Grant number: NIA #AG05138.

*Correspondence to: Brent A. Vogt, Cingulum NeuroSciences Institute, 800 Irving Ave., Syracuse, NY 13210.
E-mail: bvogt@cingulumneurosciences.org

Received 30 January 2001; Revised 2 May 2001; Accepted 26 June 2001

Armstrong et al., 1986; Vogt et al., 1995). However, consideration of the Brodmann map suggests some disagreement with the histologic studies that place retrosplenial cortex further rostral. Brodmann also showed that cortex surrounding the splenium of the corpus callosum was retrosplenial areas 29 and 30, whereas histologic studies showed these areas in the callosal sulcus (CaS) at caudal levels.

Problems with the Brodmann map became acute when a widely used standardized atlas (Talairach and Tournoux, 1988) attempted to localize the retrosplenial areas without plotting the full depth of the CaS or its histologic features and errors were made transposing Brodmann's map to cross-sections. For example, Brodmann used a narrow width of symbols at the caudal lip of the central sulcus for area 3, suggesting it is in the central sulcus, and this has been confirmed histologically (Braak, 1980; Zilles, 1990). Although most investigators know the area 3 problem, this transposition error was repeated in all cortical regions, including the posterior cingulate gyrus, and the location of retrosplenial cortex (RSC) on the CGv is not generally appreciated. Mislocating RSC impedes imaging studies from assessing the contribution of these areas to brain functions.

The structure of each area in the posterior cingulate and retrosplenial regions is best understood in terms of the principles of cortical transition based on the evolutionary studies of Sanides (1970) and human studies of von Economo (1929), and described for posterior cingulate gyrus (Vogt, 1976, 1993; Vogt et al., 1997). Each area represents one or more transitional events, including differentiation of layers through changes in dendritic architecture and cell sizes and packing densities. Periallocortical areas have a densely granular external pyramidal layer that progresses to proisocortical areas with a weakly defined or dysgranular layer IV and which differentiates into isocortex with a well defined layer IV and large pyramidal neurons in layers IIIc and Va. Although early investigators referred to transitional area 30 (Brodmann, 1909), area LD (von Economo, 1929), or Rsag (Rose, 1928) as agranular, they did not have the modern concept of a dysgranular architecture now recognized in orbitofrontal (Hof et al., 1995), insular (Mufson et al., 1997), and anterior and posterior cingulate cortices (Vogt, 1976; Vogt et al., 1995).

The context for the present studies was defined by hypotheses from Brodmann's map and its transposition to sectional anatomy by Talairach and Tournoux (1988). The structural criteria for areas 29 and 30 on the CGv and area 23a on the cingulate gyral surface are provided in the present study and are based on previous observations in the monkey and human brains cited above. These criteria were used to determine areas forming the isthmus of the cingulate gyrus and where they abut posterior parahippocampal areas. Because the gross morphology of this cingulate subregion is not uniform, structural variants must be part of its analysis. In some instances, this cortex is thrown into a fold termed the caudomedial lobule by Goldman-Rakic et al. in the monkey (1984; CML). When an overt CML is not apparent in a human case, the term caudomedial region (CMR) is used here.

The null hypothesis is based on the maps of Brodmann (1909) and Talairach and Tournoux (1988) and states that the CML is composed mainly of periallocortical and proisocortical areas, and there is no evidence for an isocortical layer IV like that in area 23. This hypothesis was tested in the following manner: (1) Characterize areas 26, 29, and 30 on the CGv and area 23a above the splenium where their structure is established. (2) Evaluate the distribution of these areas around the splenium, including the CMR in multiple planes of section. (3) Define each area with an antibody to neuron-specific nuclear binding protein (NeuN) for determination of neuronal architecture without glial and vascular elements. (4) Evaluate immunohistochemical material above the splenium and across the CMR with an antibody to nonphosphorylated neurofilament proteins (SMI32; Nimchinsky et al., 1997; Vogt et al., 1997). (5) Evaluate the parahippocampal areas adjacent to posterior cingulate cortex to ensure the criteria for each retrosplenial area does not overlap with them. (6) Generate subregional flat maps similar to von Economo's (1929) to ensure a consistent application of histologic criteria, to assess variability for different gross morphologies, and to show the distribution of each area and borders between the cingulate and parahippocampal regions. Although a small part of area 29m occasionally appears at the rostral edge of the CML, the null hypothesis was discarded because of the robust layers IIIc and IV on the surface of the CML.

Abbreviations

CalS	calcarine sulcus
CaS	callosal sulcus
CC	corpus callosum
CCs	splenium of the corpus callosum
CG	cingulate gyrus
CGv	ventral bank of the cingulate gyrus
CML	caudomedial lobule
CMR	caudomedial region
CS	cingulate sulcus
CTPCS	common truck of the parieto-occipital and calcarine sulci
IG	induseum griseum
MR	marginal ramus of the cingulate sulcus
NeuN	antibody to neuron-specific nuclear binding proteins
NFP-ir	immunoreactive-nonphosphorylated neurofilament proteins
PHG	parahippocampal gyrus
PHGt	transitional parahippocampal gyrus
PMI	postmortem interval
POS	parieto-occipital sulcus
Pro	area properistriata
PS	parasubiculum
PSD	postsplenial dimple
RSC	retrosplenial cortex
SMI32	antibody for nonphosphorylated neurofilament proteins
SpS	splenial sulci
Sub	subiculum

MATERIALS AND METHODS

Case material

Cases were selected from a large collection of brains depending upon whether there was a complete series of sections through the entire retrosplenial and posterior cingulate cortices and excellent quality histology; i.e, uniform, dark, and well-differentiated Nissl staining and immunohistochemistry. Cases were excluded with neurodegeneration (i.e., evidence for long-standing infarcts) either in this region or in areas that project to RSC such as parahippocampal cortex. Cases in which more than 1% of the thionin-stained cortical neurons were negative for

NeuN were excluded because they may be expressing an undiagnosed, preclinical neuropathology. For example, lack of NeuN immunoreactivity in thionin-stained neurons occurs in Alzheimer's disease (Vogt and Hof, unpublished observations), and this raises concern about such a finding in "control" cases. Based on these criteria, three celloidin-embedded cases and six frozen-sectioned cases were selected. All cases were Caucasian, five were male and four were female, and none had evidence of cognitive impairments based on an evaluation of the clinical records and family reports. There was one 45-year-old man in each set; one died of a small brainstem stroke and the other in an automobile accident and there was no evidence of cortical damage in either instance. The former of these cases had a brain weight of 1,093 g and a 6-hour postmortem interval (PMI), whereas the latter had a 1,280 g brain and 10.5-hour PMI. All other cases were from elderly individuals with an average age of 73 years. Three died of carcinoma of the liver or lung, two of pneumonia, and two had an unknown cause of death and average brain weight was 1,190 g. The average PMI for five of these cases was 6.2 hours, and those for the other two are unknown.

Tissue processing

Standard methods were used and have been described previously for celloidin (Vogt et al., 1995) and immunohistochemistry (Nimchinsky et al., 1997). The entire dorsomedial surface for six cases used for immunohistochemistry were postfixed in paraformaldehyde for approximately 3 days and then placed in phosphate buffer (pH 7.4) for 1–2 weeks and taken through a graded series of sucrose culminating in a 1-week period in 30% sucrose in buffer. These medial surfaces were cut into 0.5- to 1.5-cm blocks. One entire brain for celloidin embedding was fixed in 10% formalin for 1 year and the other two were fixed for 1 or 2 months before cutting into blocks for further processing. After fixation, the medial surface of all cases was digitally macrophotographed, cut into blocks, and then photographed again to record the limits of each block. Celloidin tissue was cut into six series at either 50 or 66 μm thick, and one series was stained with cresyl violet. The blocks for frozen sectioning were cut in a cryostat into 50-μm-thick sections in 6 or 10 series. One series was stained with thionin, and the following immunohistochemical techniques were used. All sections were preincubated in 75% methanol to block endogenous peroxidase and 25% peroxidase for 15 minutes, 3-minute pretreatment in 95% formic acid to improve reactant tissue penetration and exposed to the antigens.

The NeuN antibody identifies an unknown antigen in neurons (Mullen et al., 1992) and is ideal for cytoarchitectural studies that seek to assess differences in the size, shape, and density of neurons. In these studies, there is always the chance, particularly in layers with many small neurons such as layer IV of areas 23a and 30 or the granular layer of area 29, that nonneuronal elements interfere with the conclusions. Use of NeuN essentially eliminates glial and vascular elements from the analysis. Wolf et al. (1996) could find no evidence of nonneuronal staining in human postmortem cortex and Eriksson et al. (1998) found no evidence of cross-reactivity between glial fibrillary acidic protein and NeuN immunoreactivity in developing human hippocampus. In adult human cortex, only Cajal-Retzius cells in layer I are not labeled with NeuN (Sarnat et al., 1998). To monitor the efficiency of NeuN immunoreactivity, sections were counterstained with thionin. The counterstain ensures that no alteration in antigen expression goes undetected, i.e., cases with many thionin-stained neurons that were NeuN negative were excluded as noted above. The counterstain also provides the opportunity to consider the density and distribution of blue-stained glial and vascular elements in the context of the heavily immunoreacted neurons in each layer. For example, neurons and glia in layers II and IV were evaluated in this manner.

The NeuN antibody (Chemicon, Temecula, CA) was used at a 1:1,000 dilution. Vectastain Elite Mouse ABC Kit (Vector Labs, Burlingame, CA) was used with 3,3′-diaminobenzidine tetrahydrochloride (DAB) as the horseradish peroxidase substrate. Expression of nonphosphorylated epitopes on the medium (168 kDa) and heavy (200 kDa) molecular weight subunits of the neurofilament triplet protein was analyzed with the SMI32 antibody (Sternberger Monoclonals, Lutherville, MD). It was used at a 1:10,000 dilution and then reacted with the Vectastain Elite Mouse ABC Kit and DAB, mounted, and counterstained with thionin. Specificity of the immunoreactivity was verified by performing the reaction without primary antibody in each case.

Data analysis

Cytoarchitectural studies that use Brodmann's numbering scheme and variations thereon begin with analysis of the architecture of the center of each area (centroid analysis) to ensure that his intentions are understood in terms of the structure and location of each area and are not confounded by the structure of adjacent cortices. Although Brodmann did not document each area photographically, he used classic methods such as Nissl staining in celloidin-embedded tissue and this is where the present analysis begins. The areas considered in a first pass, microscopic analysis through the Nissl and NeuN series for each case were as follows: posterior cingulate areas 31, 23a, 23b; ectosplenial area 26; retrosplenial areas 29 and 30; parahippocampal areas 27, parasubiculum (PS), 35, and 36. In some instances, we were unable to identify a uniform area during the first pass and it was subdivided further. Granular area 29 has a lateral division (29l) and a medial division (29m). In addition, we were unable to show that caudal area 36 is equivalent to much of its rostral counterpart. This transition cortex is termed area 36′, and it is divided further to accommodate two different structures (i.e., areas 36′d; 36′v). Once the cytoarchitecture of the center of each unique area is specified in Nissl preparations, the borders were analyzed for nonphosphorylated neurofilament protein (NFP) immunoreactivity with the SMI32 antibody. This antibody is particularly useful in midcortical layers IIIc and Va of areas 30 and 23 and IV of area 29m where there are often moderate to large, NFP-ir pyramidal neurons. This antibody is also very useful for distinguishing the dysgranular composition of area 30 and helps to determine its border with area 23a and for determining the composition of cortex in the CMR.

The analysis of each case involved testing preliminary hypotheses derived from Brodmann (1909) and our experience with the histology of these regions in primate brains. After defining each area on the ventral bank of the cingulate gyrus (CGv), CMR, and posterior parahippocampal cortex in each case, drawings of Nissl-stained sections in a 1 in 6 series of sections at 13× were made with an Aus

Jena microfiche projector. By using higher magnifications of 100–400×, each area was analyzed and its borders plotted onto the drawn sections. Examples of the center of each area were then photographed in both NeuN and SMI32 preparations for detailed analyses of the cytologic features required for localization of each area. At the end of this hypothesis-driven phase of the research, representative cases of each gross pattern of sulci and gyri were used for a flat map analysis as described below.

All documentation of histologic observations was made by taking photographs with 4 inch × 5 inch Polaroid positive/negative film (Type 55) and the negatives were scanned with a Linotype-Hell flatbed scanner. The digitized negatives were imported to Adobe Photoshop 5.2 and reversed to positive images. In some instances, photomontages were made of three to seven photographs as shown in Figures 2 and 8. These montages were merged after flatbed scanning in Adobe Photoshop 5.2. The concept of a dysgranular cortex is particularly difficult to document photographically in high magnification strips of area 30, because sampling can easily be selected for parts that have a clear layer IV or other parts that have a poorly differentiated layer IV. To overcome this sampling problem, montages of photographs were taken of layers IIIc-Va throughout the full lateral-to-medial extent of area 30 (Fig. 8) dorsal to the splenium at high magnification.

Each figure provides different levels of morphologic detail and labeling thereof. There is a macrophotograph of the posterior cingulate region, some orienting sulci and gyri are labeled, and the levels of each section marked with lines and/or arrows. In the macrophotograph, each section level is designated with a letter or an arrow is used to direct attention toward a section in the illustration. In some instances, higher magnifications of particular areas are provided and these are indicated with boxes around the magnified cortex. Around each section, there are arrows marking the borders between areas and the relevant areal designation is shown between each pair of arrows. Finally, higher magnification photographs of one or more areas are provided. In addition to labeling borders between each area, the layers are marked on all NeuN preparations, because neurons are always labeled in all layers. The SMI32 preparations are labeled mainly where there are immunoreacted neurons; layer II, for example, usually does not have NFP-ir neurons and is usually not labeled. An adjacent NeuN immunoreacted section is always provided as a guide to interpreting the SMI32 preparations. In instances where all layers are marked in the SMI32 photograph, the laminar borders are approximations based on the adjacent NeuN sections.

Because more than 50% of the cortical surface can be located in the depths of cortical sulci, flat maps are a necessary counterpart to any study of human cytoarchitecture. Subregional flat maps are preferable to those that reconstruct the entire medial surface, because the subregional maps require fewer warping steps to accommodate the unfolding procedure, i.e., they stretch the cortex in one dimension rather than two and require no oblique warping. Subregional flat maps were constructed by drawing each section at 13× and then defining the area borders microscopically and placing each on the drawn sections. A line was drawn midway between the pia and white matter borders (i.e., midcortical level) and the length of this line determined for each area. The edge of the fasciolate and cingulate gyri was then estimated from the digital images of the medial surface and drawn onto graph paper. The size and orientation of each tissue block was established and the measurements for each area used to draw a straight line for each section. Because this study was restricted to the posterior cingulate, retrosplenial, and parahippocampal areas, no further warping was applied to the sections. The warping was produced in a single posterior direction. This process resulted in a relatively precise localization of each area without alterations in other planes, and it meant that the surface area occupied by each area on the flat map was an accurate measurement of its overall area in this subregion. In the last case, there were no clear markers of the CML and Adobe Photoshop software was used to warp the flat map onto a photograph of the medial cortex. Area localization in the resulting map was consistent with multiple surveys of the histologic sections.

RESULTS

Gross morphology and structural hypotheses

The only gross structural feature in posterior cingulate cortex that consistently delineates a cytoarchitectural border is the CaS at the apposition of the ventral apex of the cingulate gyrus and the corpus callosum. This feature designates the border between area 23a dorsally and area 30 ventrolaterally. Although the splenial sulcus does not delineate an area per se, it is surrounded by area 31 and identifies most of this cortical area. All other gross anatomic features are so variable that they cannot be used to consistently identify cytoarchitectural areas.

The surface of the posterior cingulate gyrus extends ventrally to form an isthmus that abuts posterior parahippocampal cortex. In some instances, there is a tongue of cortex in this region that provides no landmarks for the transition from retrosplenial and posterior cingulate cortices to the parahippocampal gyrus (PHG). In other instances, there is a clear fold of tissue at the terminal part of the posterior cingulate gyrus. Goldman-Rakic et al. (1984) referred to this consistent and terminal part of the monkey cingulate gyrus as the caudomedial lobule (CML). When a CML is present in human cases, the common trunk of the parieto-occipital and calcarine sulci (CTPCS) appears to interrupt the isthmus to form the CML. When an overt lobule is not present, the term caudomedial region (CMR) is applied here. Finally, there are instances in which a cortical fold occurs just below the CML. Because this fold contains mainly caudal extensions of parahippocampal cortex, this is termed the transitional PHG (PHGt). The PHGt is usually not observed without dissection, because it is buried in the CTPCS.

The Brodmann map of human RSC (1909) and Talairach and Tournoux's (1988) interpretation thereof for sections through a case in standardized anatomic space provide specific hypotheses and a strategy for histologic sampling. This region in Brodmann's map is shown in Figure 1, and an oblique section taken through it; a section that is part of a case analyzed in detail below. On this section are identified the approximate location of each of the areas predicted from one interpretation of the Brodmann map. It includes a pass through areas dorsal to the splenium where Brodmann shows that area 23 forms the entire gyral surface and ventral bank of the cingulate

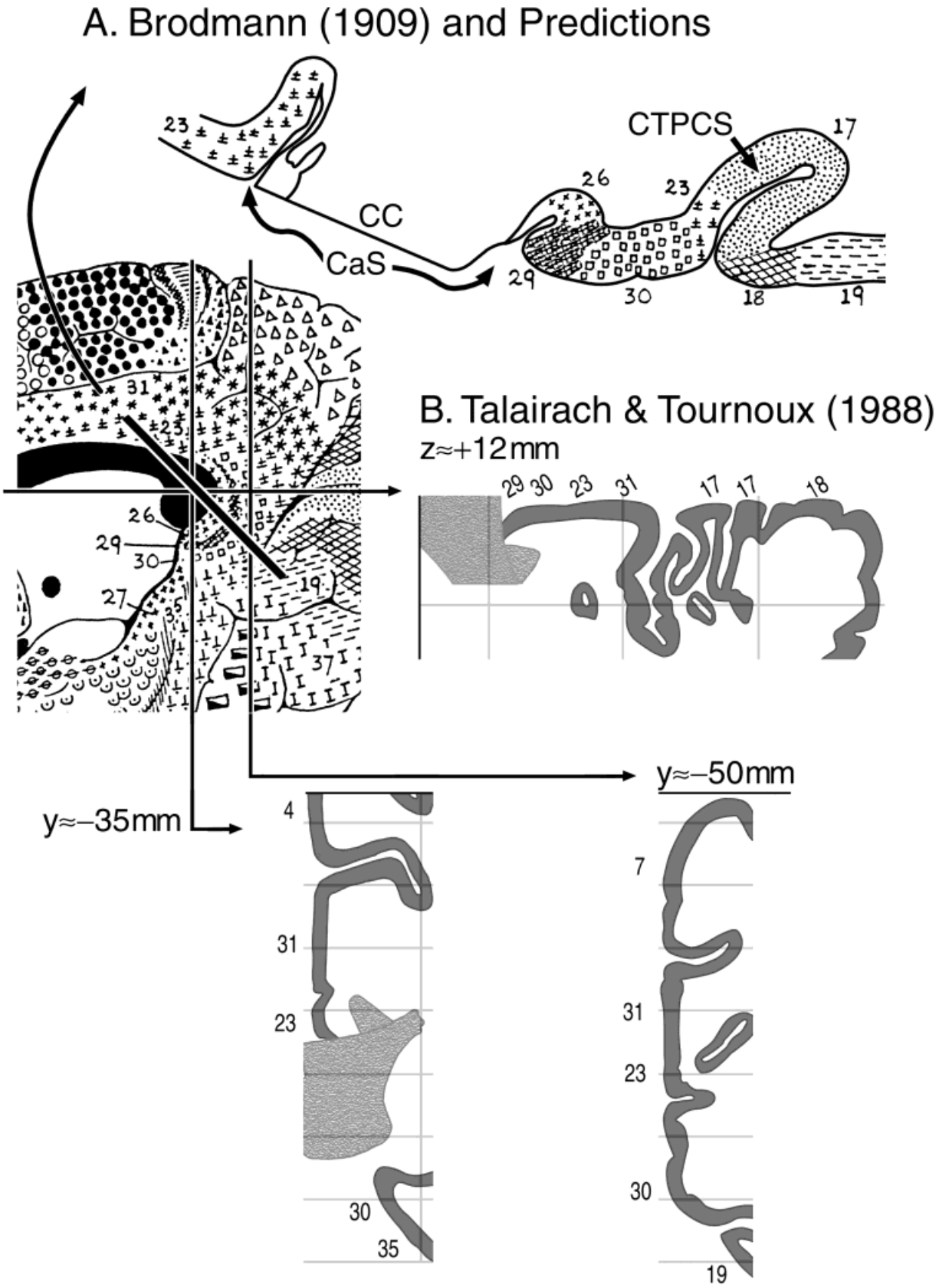

Fig. 1. The hypotheses and sampling strategies for the present study derive from Brodmann's map and its use for sectional anatomy by Talairach and Tournoux (1988). **A:** Brodmann's reconstruction of the posterior cingulate region and predictions therefrom about the distribution of areas on an oblique section through this region. An important issue is whether or not area 30 is on the CML as it appears from one interpretation of Brodmann or whether areas 29 and 30 are located in the CaS. **B:** Because Talairach and Tournoux used the prediction stated in A, that did not consider the nature of cortical folding in the posterior cingulate region, examples of transpositions made by this atlas are provided. In the horizontal section at z≈+12 mm, areas 29 and 30 are shown on the posterior cingulate gyrus as they are for coronal sections approximating y≈-35 mm and -50 mm. Notice that, at z≈+12 mm and y≈-35 mm, there is essentially no CaS represented, requiring that areas 29 and 30 be displaced to the gyral surface. For abbreviations, see list.

gyrus (CGv). One interpretation of this map is that, caudal and ventral to the splenium, most of the CMR is composed of areas 29 and 30 and a very small part of area 23. A second interpretation is that Brodmann's use of the folded cortex and narrow bands of symbols for each area suggested these areas are in the CaS and not directly exposed on the surface of the CML. The null hypothesis for the present study assumes that Brodmann intended the former interpretation of his map and it states there is no isocortical layer IV like that of area 23 in cortex of the CML. This hypothesis is consistent with the expectation that layer IV will have a dysgranular organization similar to that in area 30. In the survey of sections and photographic documentation that follows, CML cortex is analyzed in an objective effort to test this hypothesis and is based on established criteria developed by histologic studies of these areas on the CGv.

Talairach and Tournoux (1988) used the first interpretation of Brodmann's map, as discussed in the previous paragraph, to transpose each area for sectional anatomy. The null hypothesis states that their interpretation of Brodmann is correct. It should be noted, however, that they showed a truncated CaS, i.e., the depth of the CaS at the level of the splenium is approximately half its actual depth of 8–10 mm. The reduced depth of the CaS in their atlas required that RSC be placed on the gyral surface. Furthermore, area 26 is not shown in their atlas, but Brodmann indicated it is present around the entire caudal end of the splenium. Therefore, there are reasons to expect the null hypothesis might be rejected and the distribution of areas shown by Talairach and Tournoux (1988) is incorrect.

Overview of caudomedial, retrosplenial, and parahippocampal regions

One of the three celloidin-embedded cases was processed in two planes of section; left hemisphere in the coronal plane and right hemisphere in an oblique horizontal plane to optimally capture areas in the CMR in a perpendicular orientation (Fig. 2). The cytologic characteristics of each area and their distribution can be determined in either plane of section. Cortex above the splenium is shown in Figure 2A with ectosplenial area 26 and retrosplenial areas 29 and 30 lining the CGv. The dorsal of three oblique sections (Fig. 2E) shows that much of the gyral surface in the CMR is composed of areas 23a and 23b, whereas the rostral part (Fig. 2B) has posterior divisions of area 36 referred to as area 36′. Area 36′ has dorsal and ventral subdivisions and each can be distinguished cytologically from RSC as discussed below. There is a small (1.5 mm) extension of area 29m onto the rostral border of the CML in this case (Fig. 2B). Further rostrally and just ventral to the splenium (Fig. 2D), there are parahippocampal area 27, the parasubiculum (PS in figures), and perirhinal area 36. A similar topology is noted in the oblique sections from the contralateral hemisphere (Fig. 2E–G). The most dorsal of three sections (E) has parts of gyral areas 23a and 23b and a small caudal extension of area 31. Even at low magnifications in these celloidin sections, an isocortical layer IV can be seen in area 23 (E) which is not present in area 30 dorsal to the corpus callosum (A).

The problem of reconstructing RSC on the convoluted surface of the human cortex is apparent in Figure 2E. This section shows that the isocortical areas 23 and 31 directly overlie the ectosplenial and retrosplenial areas in the CaS. It is not possible to accurately reconstruct these areas without flattening the cerebral cortex to show areas in the fundus of the CaS. At a more ventral level (F), the CA1 sector of the hippocampus replaces the indusium griseum (IG) and area 29m extends onto the rostral border of the CML adjacent to areas 36′d and 36′v. Ventral to area 36′v is the area properistriata of Braak (1980) or area prostriata of Sanides (1970; Pro in Fig. 2B,F). Area properistriata is a rostral visual area that is thin in relation to parahippocampal and cingulate areas. Striking findings of this case are that RSC does not completely surround the splenium of the corpus callosum and area 30 does not extend onto the CMR as suggested by the maps in Figure 1.

The reconstruction problem of the posterior cingulate region is emphasized once more in Figure 3A where an immunohistochemical preparation of NeuN is shown for a coronal section through the CML. As discussed in detail in the Materials and Methods section, most glia and vascular elements are not immunoreactive for this antigen and the laminar architecture is clearer in these preparations than in those stained for Nissl substance; even at low magnifications. Thus, the isocortical layer IV of areas 23a and 23b can be seen in cortex on the surface of the CML, whereas areas 29 and 30 underlie this cortex in the depths of the CaS and do not express a fully differentiated layer IV. The problem presented by this region is that it is impossible to accurately reconstruct it on the convoluted surface because cortical folding doubles the extent of cortex around the splenium. This figure also clarifies one of the important interpretations of Brodmann's map. His reconstruction reflects the ectosplenial and retrosplenial areas in the CaS and not on the surface of the CML. These observations, along with the detailed structure of cortex in this region provided below, led us to reject the null hypothesis, to conclude that Brodmann used narrow bands of symbols for each ectosplenial and retrosplenial area because they are located on the CGv, and to infer that the placement by Talairach and Tournoux (1988) of area 30 as a primary component of the CMR is incorrect.

Allocortex and ectosplenial area 26

Every section through RSC includes a segment of allocortical hippocampus and the ectosplenial area 26. Above the splenium, the hippocampal rudiment, indusium griseum (IG), or areas Lβ2 and HF (von Economo and Koskinas, 1925), is a single layer of densely packed ganglion cells that are heavily NFP-ir (Fig. 4: SMI32). Adjacent to the IG is the subicular rudiment (Sub) or area HE of von Economo and Koskinas, which has many fewer and more dispersed neurons. These two areas together form the fasciolate gyrus on the dorsal surface of the corpus callosum.

Area 26 of Brodmann (1909), area LF of von Economo and Koskinas (1925), and area "es" of Braak (1979) has an architecture that is almost the inverse of that expressed by the IG and subicular rudiment. As shown in Figure 4, area 26 has a very dense layer of granular neurons, many of which are NFP-ir, and there is a dense plexus of NP-ir fibers in this layer. Deep to this granular layer, there are few pyramidal neurons, some of which are NFP-ir (compare NeuN and SMI32 in Fig. 4). Braak (1979) observed that this layer was composed of only the multiform layer VI.

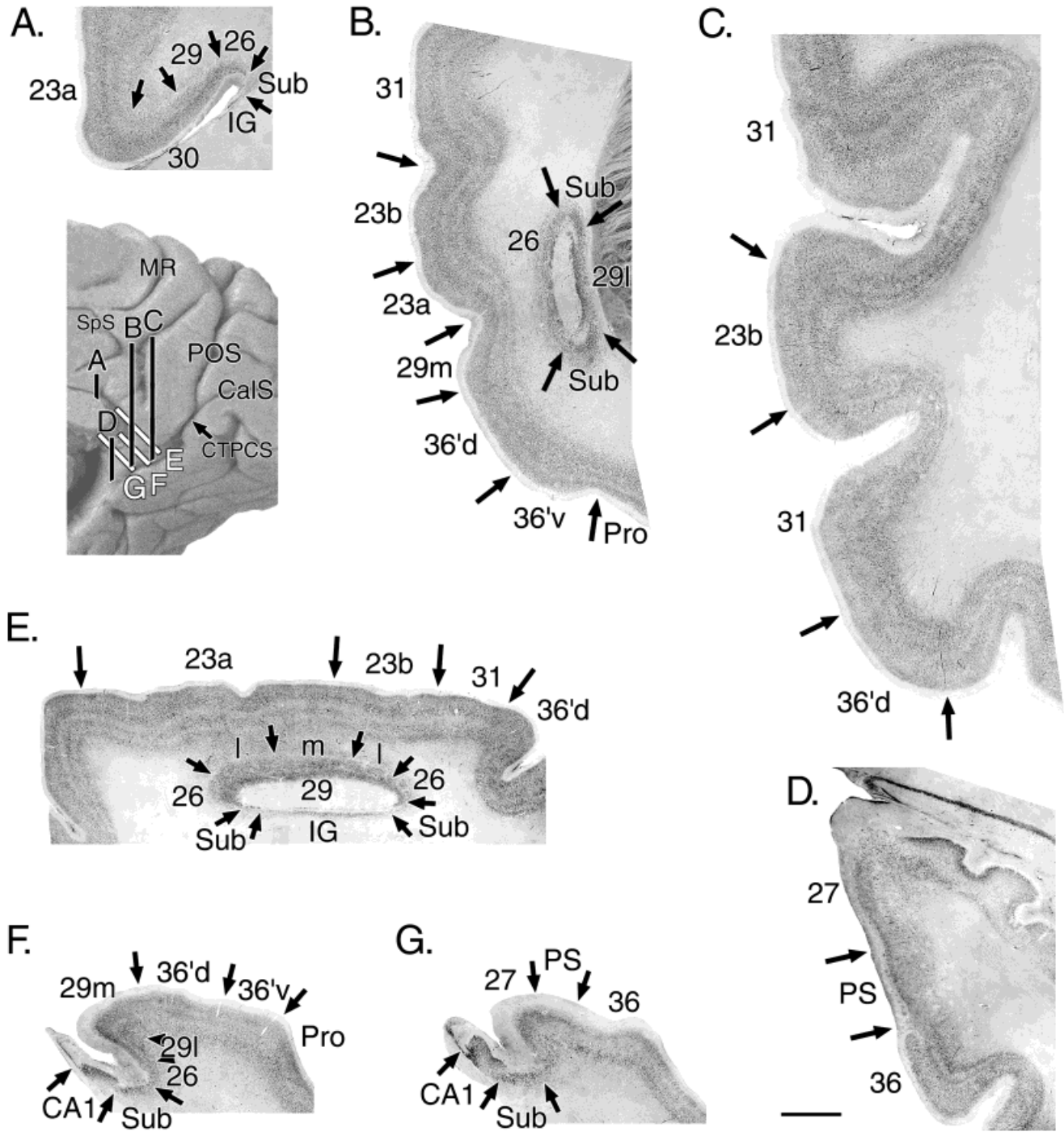

Fig. 2. Coronal (**A–D**; left hemisphere) and oblique, horizontal (**E–G**; right hemisphere, shown for orienting levels) sections from the posterior cingulate and parahippocampal regions of a celloidin-embedded and Nissl-stained case. Sections B–E are montage reconstructions from three photographs each. A: Although there is an extension of area 29m onto the rostral edge of CMR (B), areas 23a, 23b, and 31 compose much of the surface cortex. Ventrally, there are modifications of parahippocampal area 36 termed area 36′. The reconstruction paradox of RSC is apparent in B and E where the RSC underlies the CMR, indicating that accurate reconstructions of this region cannot be produced on the convoluted brain surface. In section F, the small rostral extension of area 29m onto the rostral edge of the CMR is apparent as is the first enlargement of the CA1 sector of the hippocampus. Section G shows a complete replacement of RSC by area 27 and the parasubiculum (PS) just ventral to the splenium. For abbreviations, see list. Scale bar = 2 mm in D (applies to A–G).

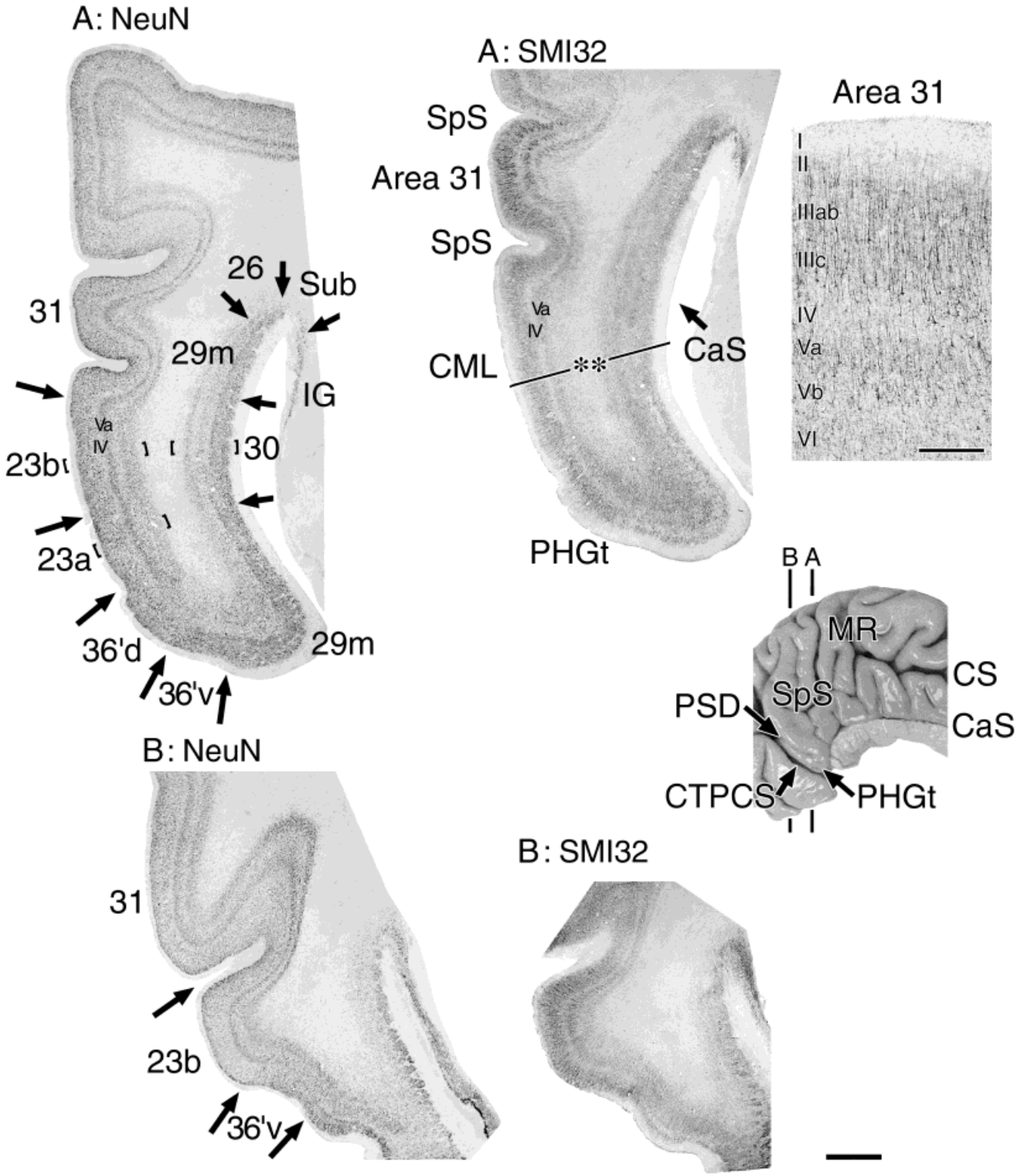

Fig. 3. Photomicrographs of immunohistochemical preparations through the posterior cingulate region and its junction with the PHG. The reconstruction paradox of RSC is clear because it is in the depths of the CaS lateral to the CML. The isocortical nature of areas 23a and 23b with their layer IV is apparent in both NeuN and matched SMI32 preparations (**A**). As is true for all cingulate areas, layer Va is prominent even in isocortex as labeled in A. These sections also demonstrate the clarity with which each area of the CML can be assessed in standard coronal sections. Although area 29m does not appear on the CML in this case, its border with parahippocampal area 36′d on the PHGt is demonstrated. Area 31 not only has the thickest layer IV of any cingulate area, it also has the highest level of NFP immunoreactivity in layer III as shown in the area 31 photograph of the SMI32 preparation. The line with a double asterisk in A: SMI32 shows the level below which sections were enlarged for Figure 6. The sections from **B** are caudal to those in A and show area 31 descending caudal to area 23b to form the most caudal part of the CML. For abbreviations, see list. Scale bars = 2 mm in B (applies to A,B), 400 μm for area 31.

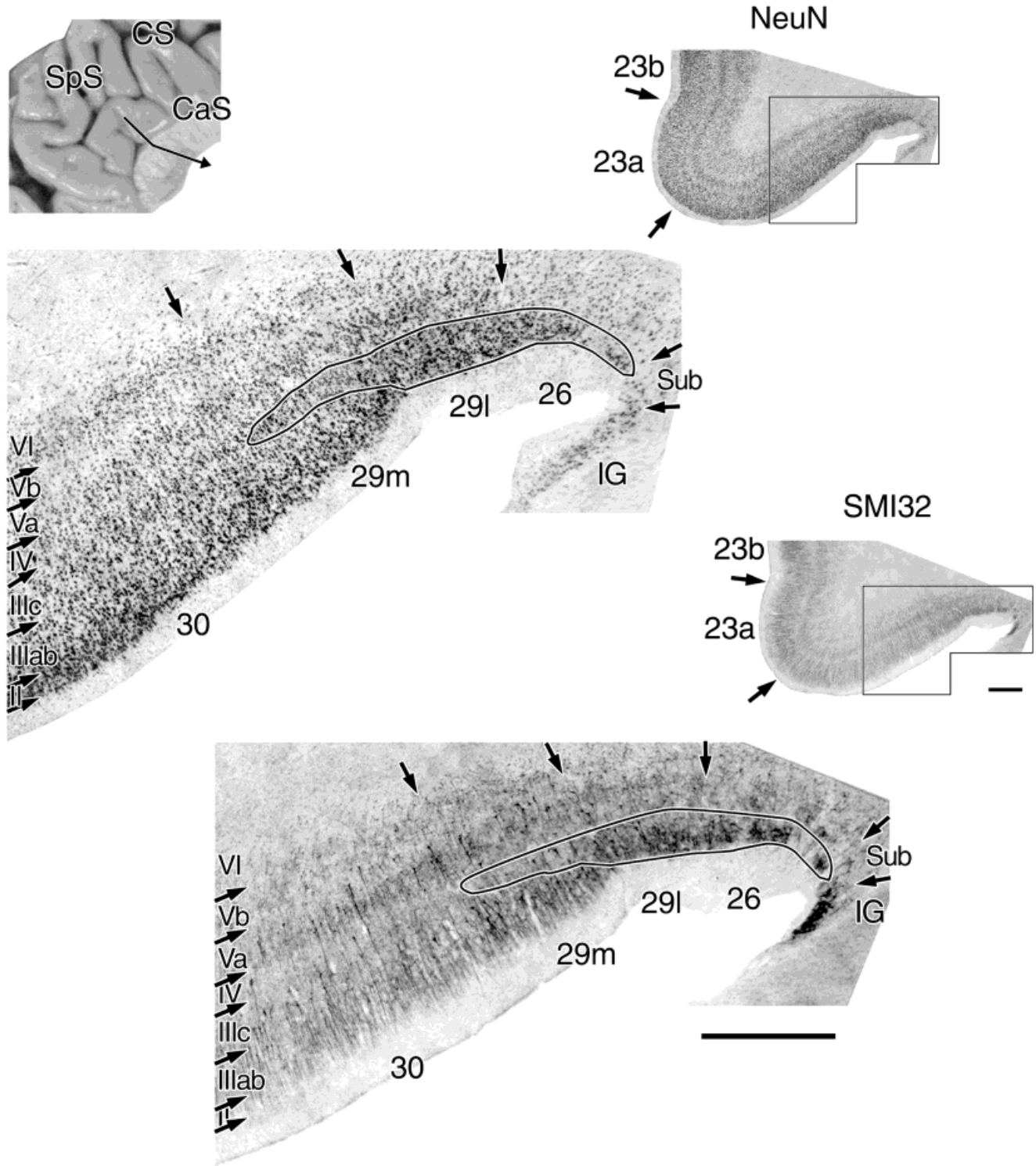

Fig. 4. Coronal sections of posterior cingulate and retrosplenial cortices dorsal to the splenium (level indicated with the line and arrow) immunoreacted with the NeuN and SMI32 antibodies. A low-magnification orientation photograph is provided with a polygon that selects the field for highest magnification photography. The sections are separated by approximately 300 μm, and they show the composition of areas on the CGv. The granular layer of areas 26 and 29 is outlined to emphasize the commonality of this layer to the ectosplenial and granular retrosplenial areas. Note that the overall density and sizes of neurons in this granular layer in area 29m is reduced because large neurons in layer III of area 29m separate from the granular layer. In area 26 of both preparations, there are almost no neurons below the granular layer, i.e., there is essentially no internal pyramidal layer. Each layer in area 30 is shown to the left, including a variable layer IV. Notice the prominent continuity of the granular layer of areas 29m and 30 in low- and high-magnification photographs of the SMI32-immunoreactive section. For abbreviations, see list. Scale bars = 1 mm.

Granular area 29

Although the general architecture of RSC can be identified in Nissl-stained preparations as in Figure 2, the details of cytologic organization are more clear with immunohistochemistry such as in Figures 3–8. Figure 4 shows a suprasplenial level of area 29. The unifying feature of its two subdivisions is the granular layer, which, in lateral area 29l, is directly adjacent to layer I, and in medial area 29m it is deep to a layer of medium pyramidal neurons. These latter neurons are in a layer termed layer III which contains neurons that have homologies to layer IIIab in adjacent area 30. The granular layer is referred to as layer III/IV in area 29l, because it is an intermediate stage of differentiation of layers III and IV on the CGv. The granular layer contains many small and medium pyramids that are NFP-ir, and the associated plexus is prominent in Figure 4. In area 29m, the density and sizes of neurons is reduced in layer IV, because many medium neurons are separated from this layer into layer III (Figs. 4, 5). Beneath the granular layer in area 29l are poorly differentiated layers V and VI, whereas in area 29m layer V differentiates into layers Va and Vb. Many of the largest pyramids in area 29 are NFP-ir, and they are located mainly in the deeper part of layer V in area 29l and the deeper part of layer Va in area 29m. Finally, there are some NFP-ir neurons in layer VI throughout area 29, although the associated plexus in layer VI is much less dense than in layers IV and Va.

The details of area 29m architecture are shown in Figure 5 adjacent to area 30. The parvocellular layer IV not only contains small and medium pyramidal neurons, it also contains several large and solitary pyramids. These neurons are NFP-ir and are a distinguishing feature of area 29m along its full extent to its termination on the rostral bank of the CML. Photomicrographs of area 29m are shown in Figure 5 and examples of three of these pyramids are emphasized with arrowheads in both the NeuN and SMI32 preparations. At his magnification, it is also clear that layer III of area 29m is composed of many medium and large pyramids that are heavily NFP-ir. These neurons likely are the undifferentiated counterparts of pyramids of layer IIIab in adjacent areas 30 and 23a.

The relative density of neurons in layer IV of areas 30 and 29m increases around the splenium and to its termination either in the ventral part of the CaS or the rostral lip of the CML. For area 30, Figure 5C shows this increase in both NeuN and SMI32 preparations. Termination of area 29m in the CaS is shown in the pullout in Figure 6 at a level that begins at the double asterisk in Figure 3. The transition at this point is with area 36′v. The NFP-ir plexus in layers III and IV are apparent and disappear as area 29m merges with area 36′v. Area 36′v only has an NFP-ir plexus in layer V. Features of area 36′v that distinguish it from area 29m include a broad layers II-III composed of more uniform, medium pyramids; a poorly defined layer IV; and an infragranular layer dominated by a uniform layer V and a narrow layer VI. Because area 36′v is quite short in its dorsoventral extent, it is easier to assess in horizontal sections as discussed below.

Dysgranular area 30

Area 30 (Brodmann, 1909), LD (von Economo and Koskinas, 1925), Rsag (Rose, 1928), and rsm (Braak, 1979) has been thoroughly analyzed histologically. Although none of these histologic studies has shown this area to be on the gyral surface in the CMR, there are two essential issues raised by the atlas interpretations of Brodmann's map shown in Figure 1: First, does any gyral component of the CMR share cytoarchitectonic features with area 30 in the CaS? Second, how do the features of area 30 compare with those on the CML, including that area which most closely relates to area 30 (i.e., area 23a which it borders)? There are several ways to answer the first question. (1) Figure 2A shows area 30 above the splenium at a relatively low magnification in the celloidin series. The large and densely packed neurons of layer IIIc can be seen, but no layer IV is apparent. In Figure 2B, layer IV can be detected in areas 23 and 31 suggesting that area 30 is not part of the gyral surface at the isthmus. Confirmation of layer IV in the CMR is provided in Figure 3, where both the NeuN and SMI32 preparations show layer IV in areas 23a and 23b. (2) Photographs were taken along the splenium of the corpus callosum as shown in Figure 5. Both levels A and B show the variable nature of layer IV in area 30 that fulfills the definition of a dysgranular cortex. A dysgranular layer IV is one that is variable in thickness and, at points, disappears because layer IIIc and Va neurons intermingle. It is this occasional intermingling of large neurons that led to the early misconception that this is an agranular cortex and the dysgranular concept was not available to early investigators. For comparison, anterior cingulate cortex is truly agranular, because it lacks a layer IV. Finally, at the juncture of areas 30 and 29m in the depths of the CaS, i.e., lateral to the CML, there is a slightly more developed layer IV (Fig. 5C).

The second question posed above regarding the comparative features of area 30 in the CaS with cortex on the CML has been partly addressed already. In addition, Figure 7 provides higher magnifications of area 30 (Fig. 7A, NeuN and SMI32) at a level equivalent to Figure 4B. Area 30 has a layer IV that is interrupted at the pair of asterisks by a bridge of layer IIIc and Va neurons spanning layer IV (Fig. 7A, NeuN). There are some medium, NFP-ir pyramidal neurons throughout layer IV in area 30. Area 23a on the CML is selected for comparison with area 30 because no area with the architecture of area 30 could be identified on the surface of the CML and area 23a is adjacent to it throughout its rostrocaudal extent. Although there are some large layer IIIc and Va neurons that are NFP-ir in area 23a on the CML, most layer IV neurons do not express these proteins. The plates in Figure 7B are from the level in brackets on Figure 3A labeled area 23a. Area 23a on the CML has a clear and continuous layer IV. There are many more NFP-ir neurons in layer IIIc, and there are almost no NFP-positive neurons in layer IV; only an occasional large solitary pyramid can be identified in layer IV when compared with area 30. Finally, there are no neuronal bridges connecting layers IIIc and Va to the exclusion of a layer IV in area 23a, although there are occasional solitary and large neurons in layer IV. Thus, area 30 is not expressed on the CML as suggested by hypotheses derived from Brodmann's map, and this finding confirms earlier rejection of the null hypothesis based on low-magnification studies of the CMR.

To avoid confusion about the concept of a dysgranular area 30, a higher level of magnification is provided for two immunohistochemical preparations in Figure 8. Although

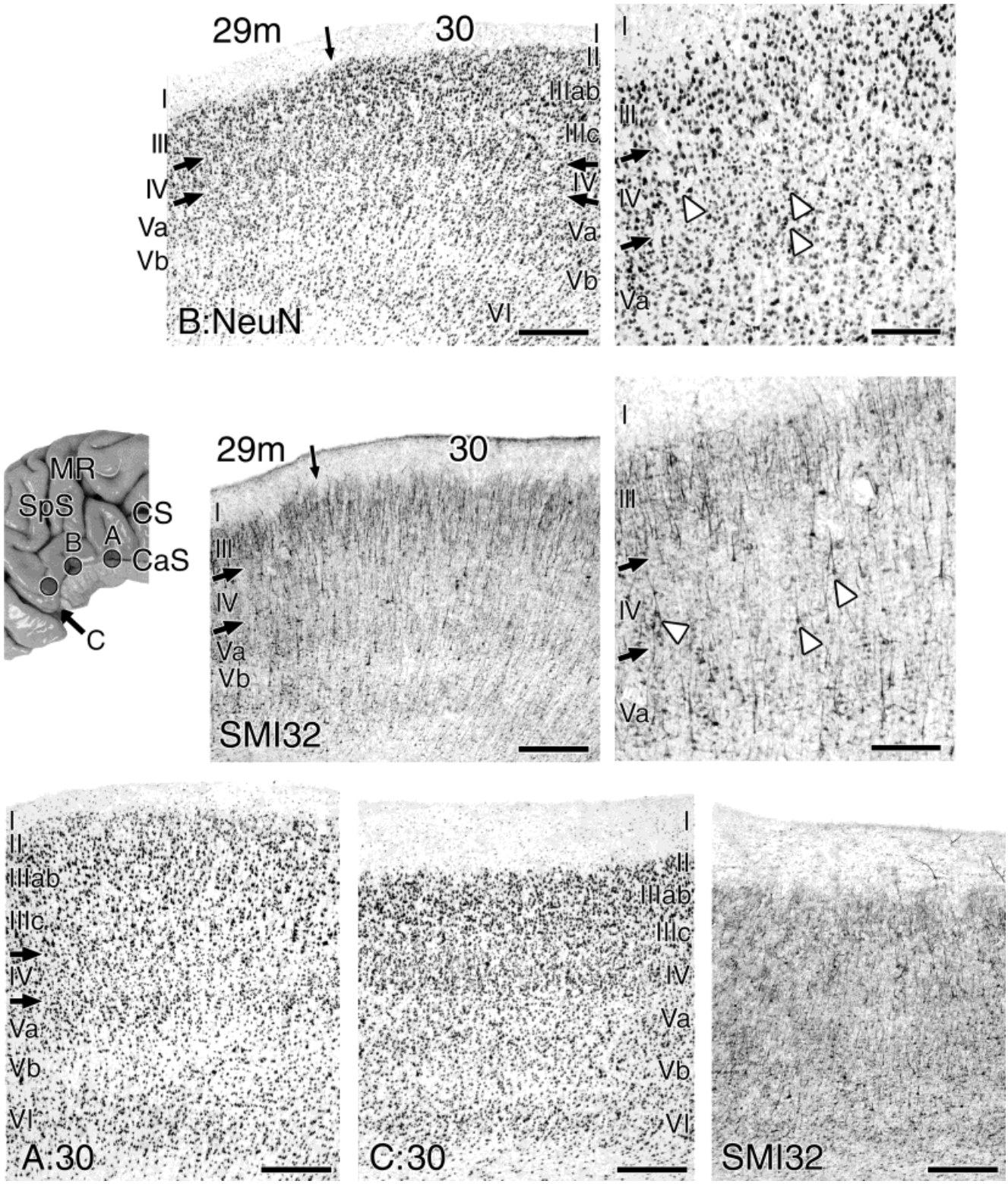

Fig. 5. Three rostrocaudal levels of area 30 above the body of the corpus callosum (**A**), dorsal to the splenium (**B**), and caudal to the splenium and lateral to the CML as indicated with the arrow pointing below the CML (**C**). The medium, NFP-immunoreactive neurons in the parvocellular layer IV of area 29m are demonstrated at high magnifications on the right where three of them are noted with white arrowheads in each preparation. Although layer IV is a variable thickness in area 30, it can be clearly identified in all three levels. The level for section C is noted with brackets in Figure 3A: NeuN. This level of area 30 is transitional to area 29m at its most caudal level, i.e., this is the terminal end of area 30. At this point, area 30 has a more densely granular layers II and IV and the sizes of layer III pyramids are reduced with less prominent NFP-ir dendrites (C:30, SMI32). For abbreviations, see list. Scale bars = 500 μm in all except for the higher magnifications in B, where they represent 200 μm.

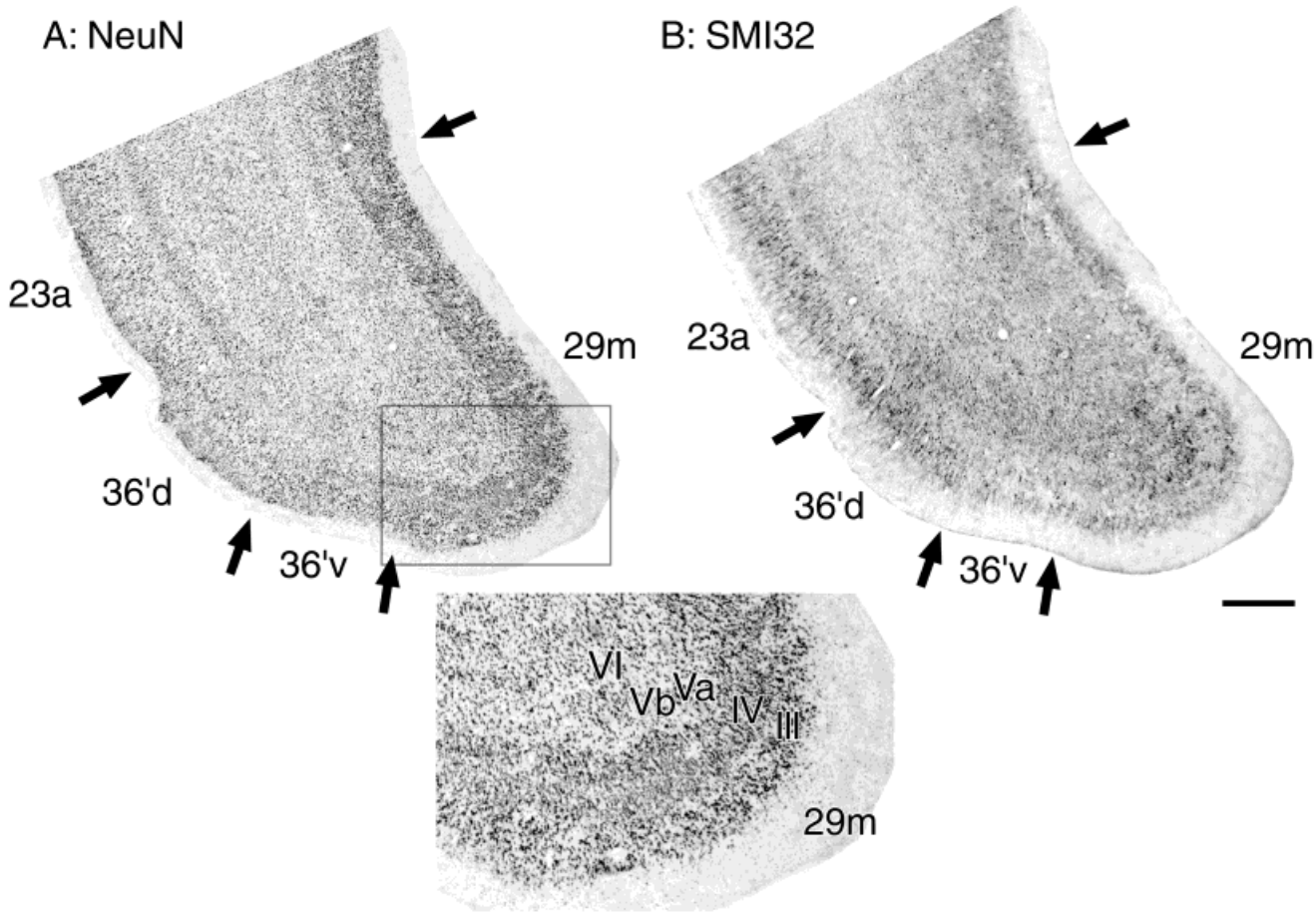

Fig. 6. Areas at the transition of the posterior cingulate and retrosplenial areas to parahippocampal cortex in coronal section. These sections are magnified from the level noted with double asterisks in Figure 3. Area 23a merges with area 36′d, and area 29m merges with area 36′v. Because the arrow between areas 23a and 36′d is also at the terminal end of the PSD, the ventral parts of these sections is the transitional part of the PHG (PHGt). The pullout of area 29m is a 2× magnification to emphasize the cytologic features of transition from area 29m to area 36′v. Scale bar = 1 mm in B (applies to A,B). For abbreviations, see list.

the dysgranular nature of area 30 in the CaS is compared with the granular organization of area 23a on the CML (Fig. 7) where the interruption of layer IV by bridging neurons is shown, it is difficult in single strips of cortex to fully appreciate the variable structure of a dysgranular layer IV. Figure 8 shows all of layer IV at a relatively high magnification in NeuN and SMI32 preparations. The NFP-ir neuronal plexuses (Fig. 8; SMI32) show that these plexuses in layers IIIc and Va of area 30 are continually separated by layer IV. Because most layer IV neurons are not NFP-ir and there are no glial or vascular elements stained, this preparation emphasizes the continuity of layer IV throughout area 30 as a negative image. However, there are breaks in layer IV by some large pyramids, and there are more medium pyramidal neurons stained in layer IV than is the case, for example, in area 23a. The bridges of large pyramids between layers IIIc and Va are noted in Figure 8 with asterisks above them in layer III. Although each of these features can be detected in the NeuN preparation, they are not as clear at this magnification.

Isocortical areas 23 and 31

To this point, it appears that the posterior cingulate gyral surface and that of the CMR are composed mainly of area 23. In this context, the most viable interpretation of Brodmann's map is that he used narrow bands of symbols around the splenium to indicate that RSC was on the CGv and extension of these areas onto the CMR was an artifact of his reconstruction technique. Figures 2 and 3 support this view in showing that a complete layer IV is in most caudomedial cortex, including areas 23a and 23b and at caudal levels area 31, whereas areas 26, 29, and 30 are lateral to the CML in the depths of the CaS.

Figures 7–10 provide examples of the structure of area 23, and Figure 7 was considered in the last section. The transition from sulcal area 30 to area 23a dorsal to the splenium is apparent in midcortical layers in Figure 8. The thick layer IV is in both preparations and the large and heavily NFP-ir pyramids in layer IIIc are apparent. Moreover, although there are NFP-ir neurons in layer Va of both areas 30 and 23a, there is a shift in the relative density with an overall reduction in area 23a. The line

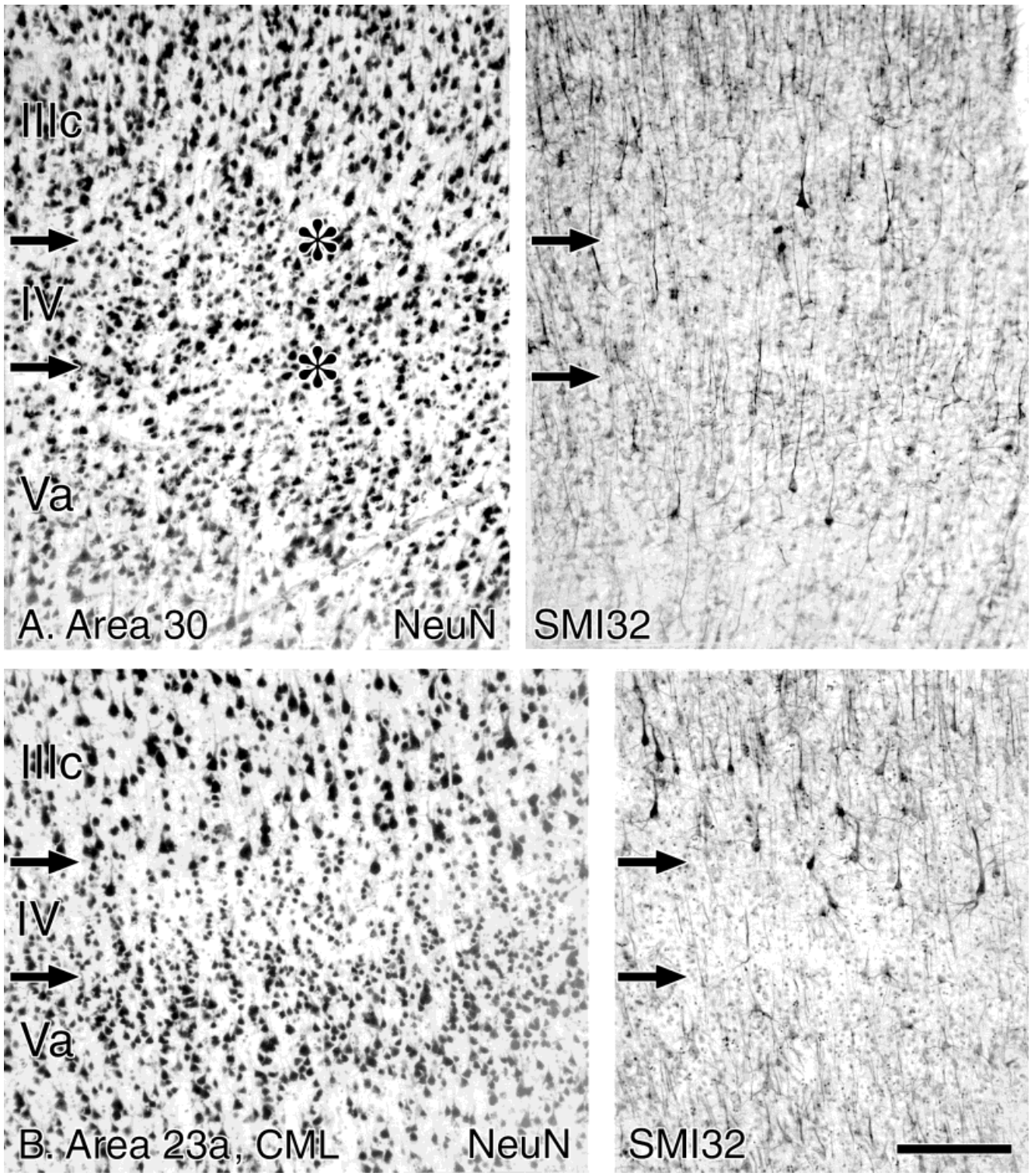

Fig. 7. Area 30 dorsal to the splenium in the CaS is compared with area 23a on the CML because no equivalent to area 30 has been identified in this latter region. These photographs were taken from coronal sections marked with brackets in Figure 3 showing the architecture of these areas without recourse to horizontal sections. The dysgranular nature of area 30 is emphasized at a point where layer IIIc and Va neurons intermingle (to the right of the double asterisks in A: NeuN). Area 30 also has a layer IV with many small and medium NFP-immunoreactive (-ir) neurons (SMI32). In contrast, area 23a has no neuron bridges over layer IV and only occasional solitary NFP-ir neurons in layer IV. Layer IIIc in area 23a has significantly larger and more dense NFP-ir neurons than is the case for area 30. For abbreviations, see list. Scale bar = 200 μm in B (applies to A,B).

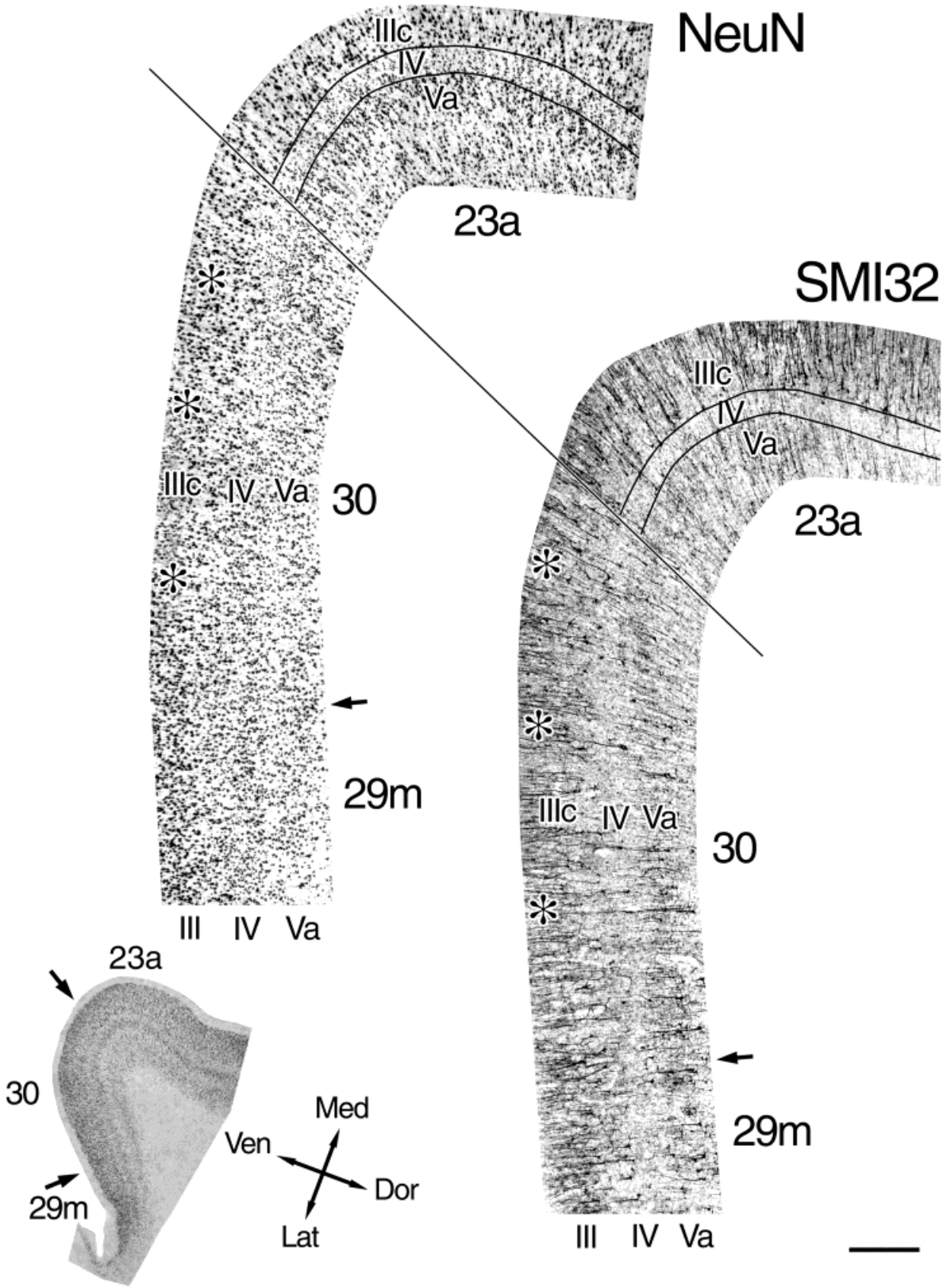

Fig. 8. The dysgranular nature of area 30 is best demonstrated with full reconstructions of layer IV rather than single strips through a sample region. These reconstructions are montages of seven photographs, each taken at an original magnification of 200×. Each montage is separated by approximately 300 μm and is from the level shown in Figure 4. The lower left insert orients the section from which the higher magnification photographs were taken (Ven, ventral; Dor, dorsal; Med, medial; Lat, lateral). A continual layer IV appears in the SMI32 preparation because of the negative-staining image, i.e., neurons that are NFP-ir in this layer are much smaller than those in layers IIIc and Va, and the plexus of these dendrites is diffuse. Variability in layer IV thickness is emphasized with asterisks at points where neurons from layers IIIc and Va intermingle. The borders of layer IV are noted for area 23a, because the layer is uniform and uninterrupted, whereas a similar outline was not made in area 30 to avoid obliterating critical morphology. The border between areas 30 and 23a is one of the clearest and most precise in the posterior cingulate region and is easily determined in both NeuN and SMI32 preparations. For abbreviations, see list. Scale bar = 400 μm.

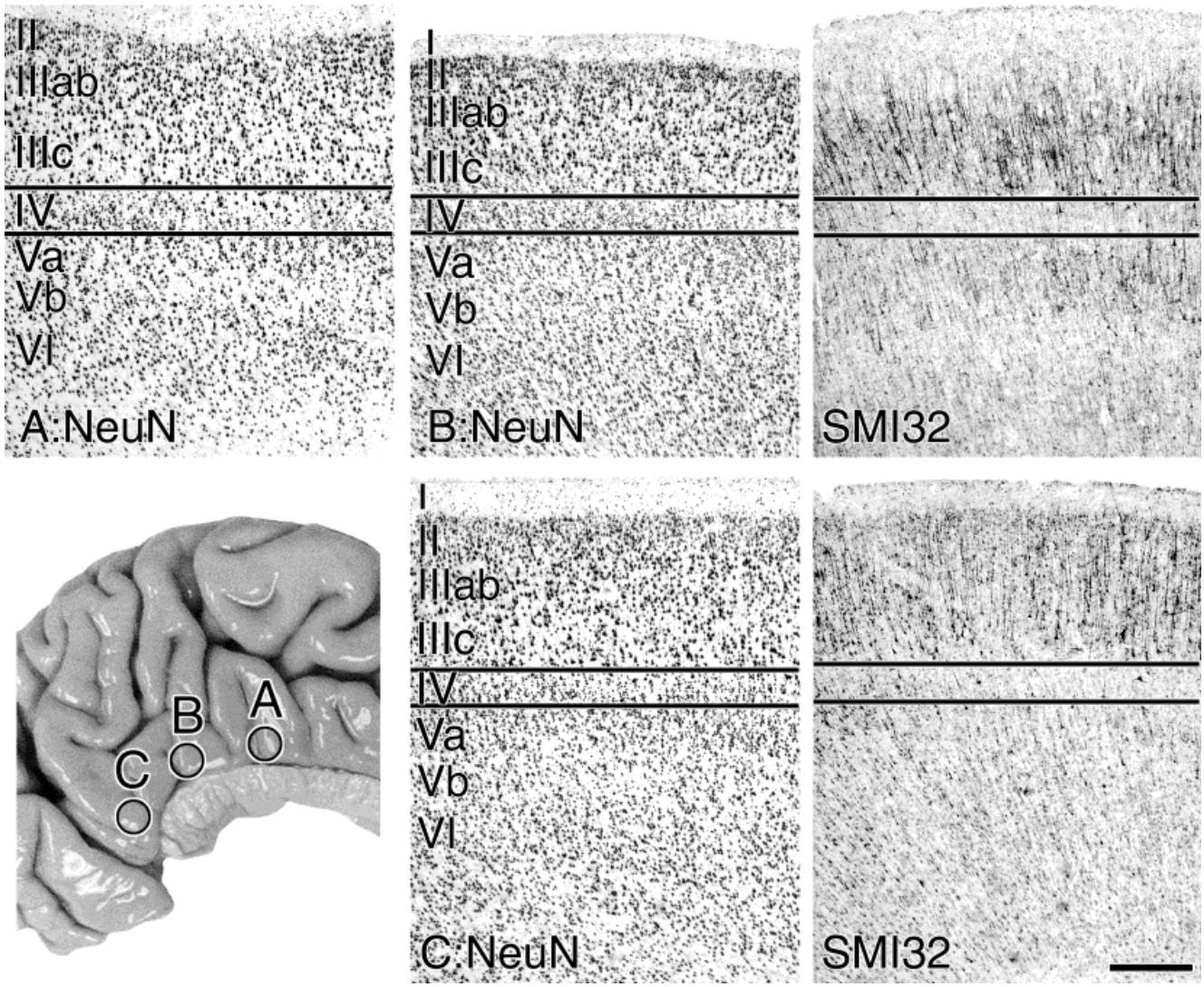

Fig. 9. **A–C:** Three rostrocaudal levels of area 23a are shown to consider architectural variability dorsal to the corpus callosum and on the CML. Layer IV has a relatively uniform thickness throughout, although there is some variation in the number of large, NFP-immunoreactive layer III pyramids, which are greatest in level B above the splenium. Level C was selected as an explicit test of the hypothesis that areas 29 and 30 compose most of the CML as suggested by Talairach and Tournoux (1988) and shown in Figure 1. This area does not have the properties of either area 29 or 30. For abbreviations, see list. Scale bar = 500 μm.

through both sections in Figure 8 makes the point quite dramatically that the border between these areas is very distinct, and it is one of the few instances where cytoarchitectural divisions can be made with the precision of as little as a few hundred micrometers.

It is possible that area 23a varies significantly in its rostrocaudal extent, and this could cause confusion about its cytoarchitecture and relations to area 30 in the CMR. Figure 9 shows area 23a at 3 rostrocaudal levels to consider this issue. At its midpoint (Fig. 9B), there is a clear layer IV with almost no NFP-ir neurons. This finding is true for the same area at rostral and caudal levels, and it can be said that area 23a is never dysgranular. Although there are more NFP-ir neurons in layer IIIc of supraplenial cortex than that on the CML (Fig. 9C), this difference alone does not produce a qualitatively different cytoarchitectural profile that could be construed as area 30, particularly in light of the heavy NFP-ir of layer Va neurons in area 30 that does not occur in area 23a.

Another major component of the CMR is area 23b. This area has such a well-defined layer IV that it is easily determined at low magnifications as in Figure 2B,C,E and Figure 3A,B. In Figure 3A,B, for example, both layers IV and Va are well defined and the transition from area 23a to area 23b is apparent (Fig. 3A) where both layers are thicker in area 23b in both immunohistochemical preparations. These are the two most important features of area 23b; thickness and neuron densities in layers IV and Va. Many large pyramidal neurons in layer Va, most of which are NFP-ir, easily distinguish these areas. These features are particularly prominent at caudal levels of area 23b (Fig. 10C, NeuN and SMI32). As is true for area 23a,

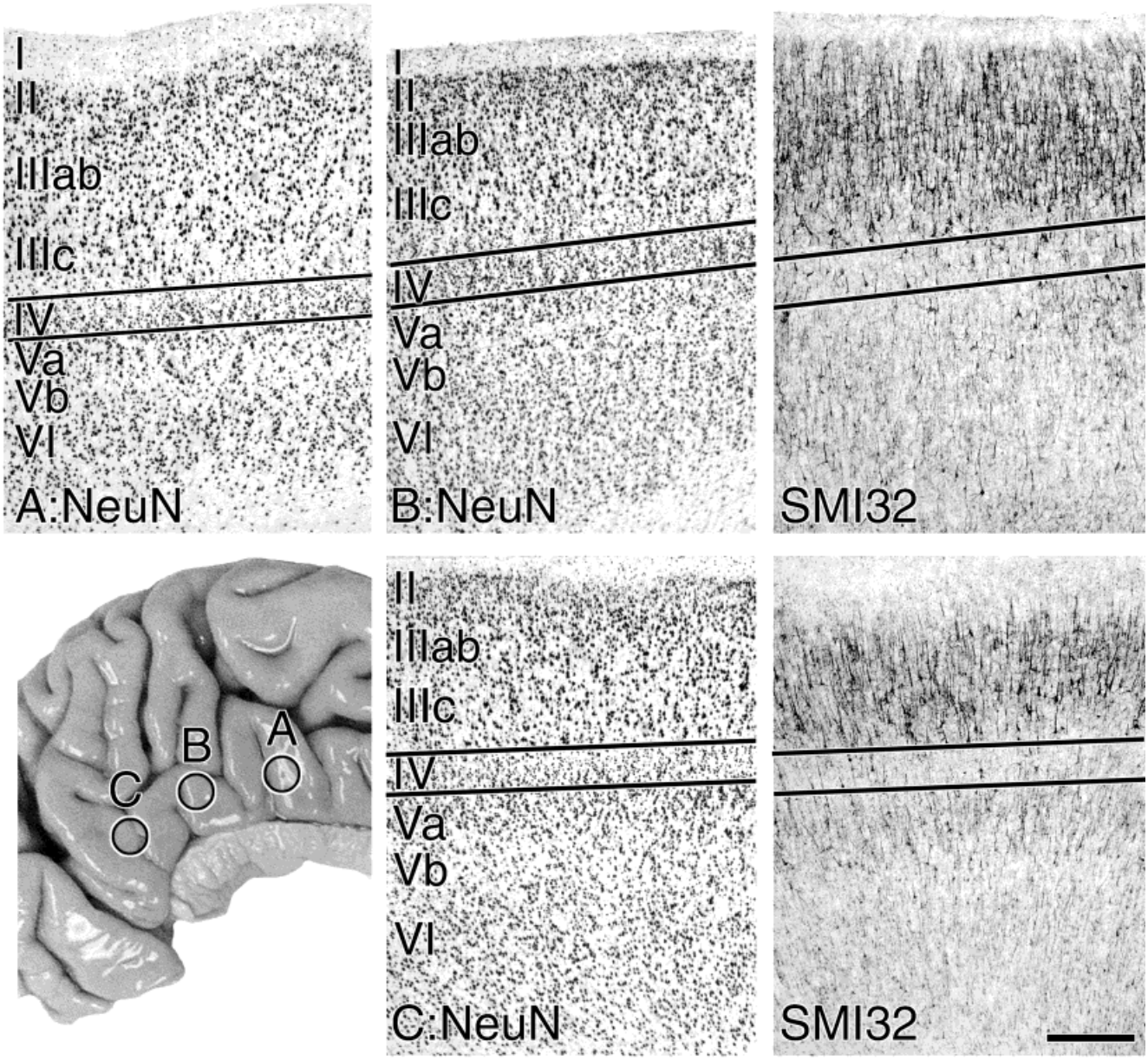

Fig. 10. **A–C:** Three rostrocaudal levels of area 23b, including a level at the dorsal part of the CML (C). Although the essential structure of area 23b is maintained throughout with a heavily NFP-immunoreactive (-ir) large neurons in layer III, thick layer IV, and robust layer Va with few NFP-ir neurons, the thickness of layer IV does decline as the border with area 24′ is approached (**A**) as is also true for area 23a in the previous figure. Notice once again that there is a very clear layer IV in both NeuN and SMI32 preparations at level C just dorsal to the CML. For abbreviations, see list. Scale bar = 500 μm in C (applies to A–C).

rostral levels of area 23b have a relatively more slender layer IV (Fig. 10A). Finally, the distinctions between areas 23a and 23b are enhanced by the extensive size and number of NFP-ir neurons throughout layers IIIab and IIIc. Although caudal levels of area 23b may have a somewhat thinner layer II overall, the relative intensity of the NFP-ir neurons is quite obvious in Figure 10B,C as well as in Figure 3A,B: SMI32.

To ensure that cortex on the cingulate gyral surface dorsal to the splenium is similar to that caudal to the splenium, Figure 11 shows photographs from each area matched for their location in relation to the dorsal edge of the corpus callosum in another case. Layers IIIc-Va are shown at a high magnification because these are responsible for the critical differences between each area, and area 31 is shown to calibrate the maximal thickness that layer IV reaches in posterior cingulate cortex. Comparison of each pair of photographs (B/E; C/F; D/G) confirms that these are the same areas above and behind the splenium. This case was used below to flat map the postsplenial subregion of cingulate cortex because it has a clear CML and PHGt.

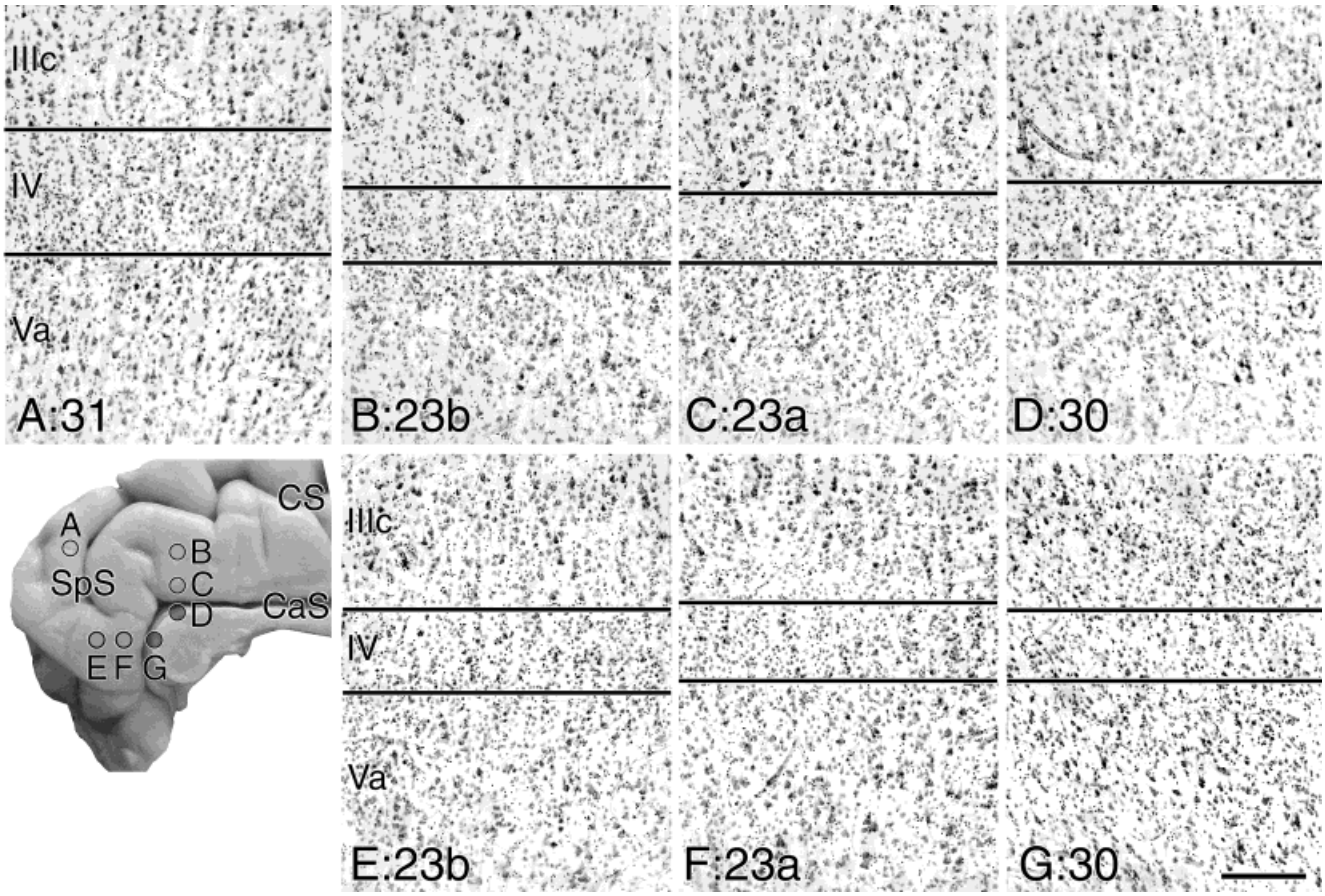

Fig. 11. **A–G:** A comparison of layers IIIc-Va of areas 30, 23a, and 23b above the splenium with the same areas caudal to the splenium, i.e., the dorsal edge of the CML. The photomicrograph of area 31 (A) provides a calibration for the greatest thickness attained by layer IV in this case in cingulate cortex. There is no apparent difference between comparable areas at these two levels of cingulate cortex (i.e., between B/E, C/F, and D/G). For abbreviations, see list. Scale bar = 200 μm in G (applies to A–G).

Although most of area 31 surrounding the splenial sulci (SpS) is not currently being considered, it does extend caudally and ventrally to enclose area 23b and form the most caudal part of the CMR. Figure 11 shows layers IIIc-Va for area 31 in comparison to different levels of area 23b and emphasizes its thick layer IV. Figure 3 shows a strip of area 31 and its massive population of NFP-ir neurons throughout all of layer III and to a lesser extent in layer Va. Each of these features serve to mark a clear boundary of area 31 with area 23b.

Posterior parahippocampal area 36′

Ventral to posterior cingulate and retrosplenial cortices are two divisions of posterior parahippocampal cortex that share features with area 36. Area 36 has well-defined layers II and Va and a dense layer VI. Layer III is broad, and the pyramidal neurons are relatively uniform in size (Fig. 2D,G). The division of layer III into a superficial layer IIIab and deeper layer IIIc is possible, although the neurons in layer IIIc do not reach the size and dispersion characteristic of the cingulate neocortical areas (Fig. 12F).

In contrast to area 36, area 36′d has a less-differentiated layer III (i.e., no ab/c divisions) and differentiation with layer II is less apparent (Figs. 2C,E, 12D). Layer Va is present but not at the clarity seen in area 36. Area 36′v is more homogeneous overall (Figs. 2B,F, 12E) with more differentiation in layer II and a more homogeneous distribution of neurons in layers III-VI. NFP immunoreactivity in these two areas can be compared in Figure 3A: SMI32. Area 36′d has a dense plexus of dendrites and neurons in layer III and a smaller one in layer Va, although this is broader than its equivalent in areas 23a and 23b. Area 36′v, in contrast, has only a narrow plexus of SMI32-ir dendrites and neurons in layer III, whereas that in layer V is much broader than in area 36′d.

Subregional flat maps

Cytoarchitectural studies of human cortex require flat map reconstruction of the areas identified because 50% or more of the cortical surface is in the sulci and this is true for the posterior cingulate region. One of the problems interpreting Brodmann's map (1909) is his use of the convoluted medial surface rather than an unfolded counterpart for a single brain. A flat map of the entire cingulate gyrus has been rendered in which the depths of the CaS are represented and areas 29 and 30 are plotted on the CGv (Vogt et al., 1995). As is true for flat maps of the entire brain, however, flat maps of the entire cingulate

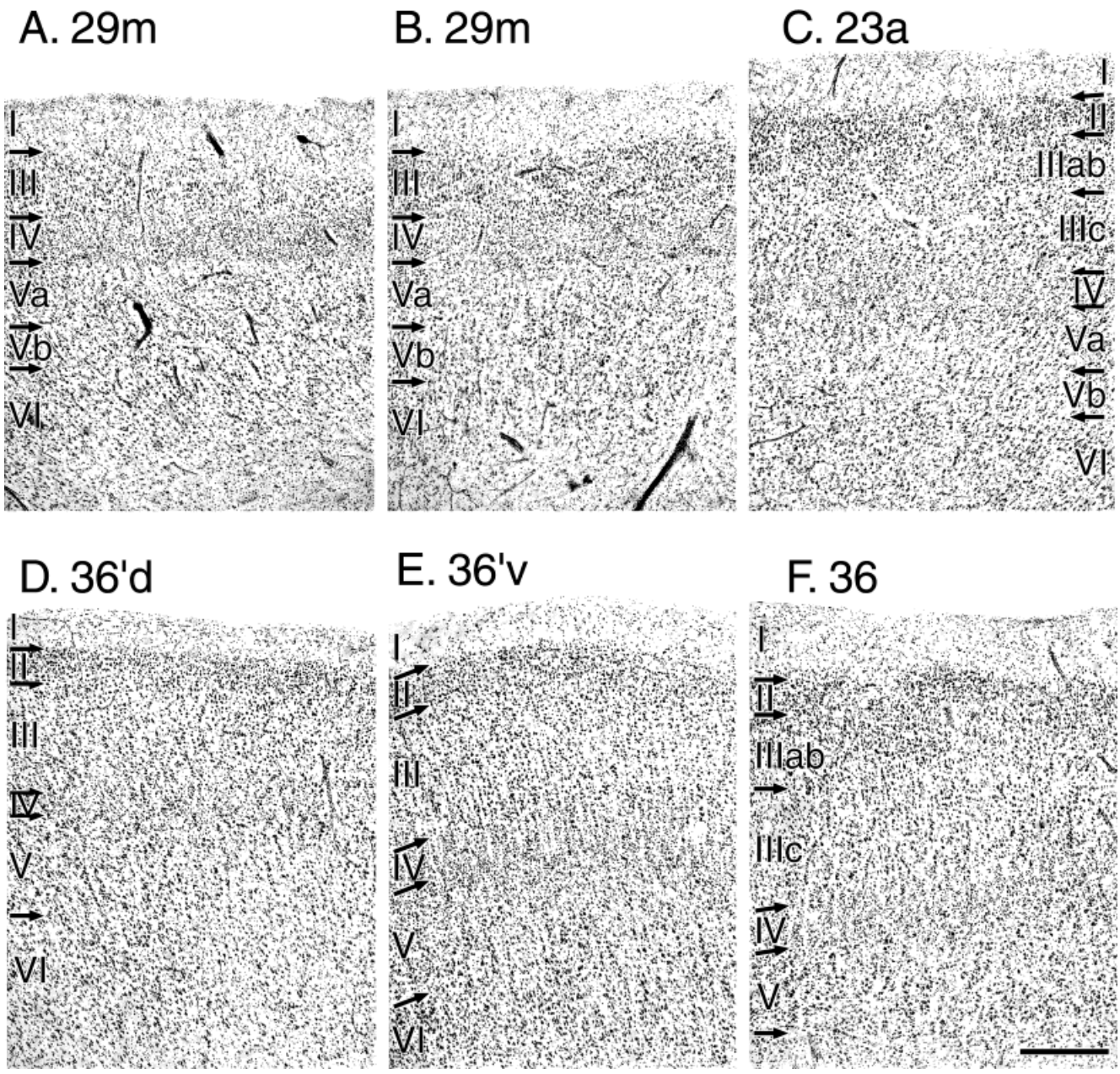

Fig. 12. **A–F:** Photomicrographs through different parts of areas on the CGv, CML, and PHGt as noted with dots and A–F in Figure 13. The similarity of area 29m in the CGv and the PHGt is shown in A and B, respectively. **C:** Another explicit demonstration of area 23a on the CML. Finally, there is a comparison of the architectures of each division of caudal area 36′ and area 36 showing the former have a less differentiated layer III. Area 36′d has a thinner layer IV than area 36′v and somewhat larger neurons in layer V. For abbreviations, see list. Scale bar = 500 μm in F (applies to A–F).

cortex result in significant distortions in all areas due to the need to warp all areas to fit a two-dimensional space and still retain basic gross morphologic relationships. Subregional flat maps alleviate this problem, because they are limited to a subsector of cingulate cortex, flattening is performed in only one direction rather than two, and it is not influenced by flattening in other parts of cingulate cortex to form a full map. von Economo (1929) provided the first subregional map of the posterior cingulate gyrus, although it was not a flattened surface. Subregional flat maps were produced in the present study for two cases: one with a clear CML and PHGt and another in which the isthmus was formed by a relatively uniform tongue of cortex without an apparent lobule.

Figure 13 shows a case in which postsplenial cortex was sectioned in the plane of the flat map reconstruction. Asterisks on the convoluted surface on the right are used to orient the flat map at the left. The first one is at the CaS and emphasizes that flattening was started at the depths of the CaS, whereas the second asterisk shows the rostral

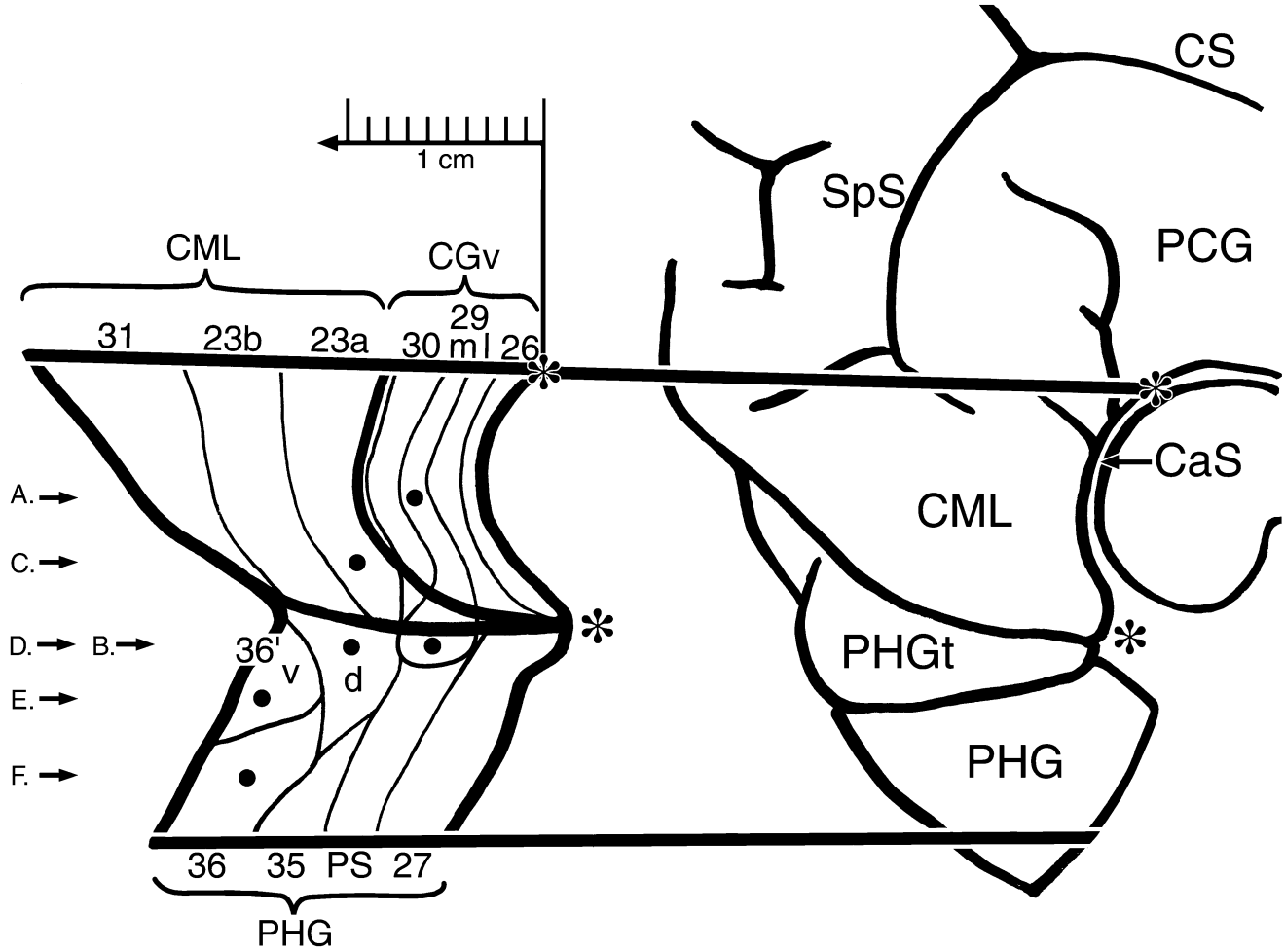

Fig. 13. Subregional flat map of cortex caudal to the splenium, including the entire CML. This is a linear expansion of posterior cingulate and parahippocampal cortices in a single direction noted by the large arrow on the scale bar (i.e., caudal from the fundus of the CaS). The dorsal asterisk in the drawing on the right extends from the depths of the CaS to an equivalent starting point on the flat map on the left and the same is true for the rostral edge of the PHG/PHGt. Areas on the CGv are enclosed by thick lines on both sides of the callosal sulcus, whereas those on the gyral surface are extended to the right on the CML. The locations and interrelationships of RSC and transitional parahippocampal areas are clear in this case with a PHGt. The A–F designations with arrows point to dots where photomicrographs were taken for Figure 12. For abbreviations, see list.

edge of the PHGt in both drawings. The depth of the CaS was determined according to the curvature of the splenium, and each area represented according to the length of the midcortical line. Heavy lines in Figure 13 represent cortex on the CGv, i.e., cortex in the CaS, and the caudal edge of the CML, whereas in the ventral part of the map, they represent the rostral and caudal limits of the PHGt and PHG. The direction and calibration of flattening in this case is shown with the arrow and scale bar, respectively.

This map shows that almost all of RSC is buried in the CaS. Area 30 ends just dorsal the area 29m, and this case has a small termination of area 30 on the rostral edge of the CML. Because standardized atlases based on Brodmann's map show that most of the CMR is composed of area 30, it is of interest to determine the actual extent of area 30 on the CML in this case. Because the map was produced by flattening in only one dimension rather than two dimensions, it accurately represents the relative surface area for each component of the CML and cortex on the CGv, proportions of area occupied by each cortical area can be calculated directly from the flat map. Area 30 composes 0.8% of CML (1.63 $mm^2 \div 200\ mm^2$), whereas it is 33% of area on the CGv at the level of the CML (31 $mm^2 \div 94\ mm^2$). In contrast, area 29m composes 2.8% of the rostral edge of the CML, whereas it is 26% of cortex on the CGv. Thus, both areas 30 and 29m are almost entirely located within the CaS, and all of areas 29l and 26 are in this sulcus. Finally, the PHGt contains a small rostral extension of area 29m and areas 36′d and 36′v. As noted for the case shown in Figure 3, neither area 29m or 30 appeared on the CML. Thus, area 30 does not compose a substantive part of the CML, and the null hypothesis can be rejected on the basis of a quantitative measure.

Because the primary cortical fold that forms the CML is not always readily apparent, the oblique, horizontal series was used from the case shown in Figure 2 to produce another flat map. Although all steps in the procedure were

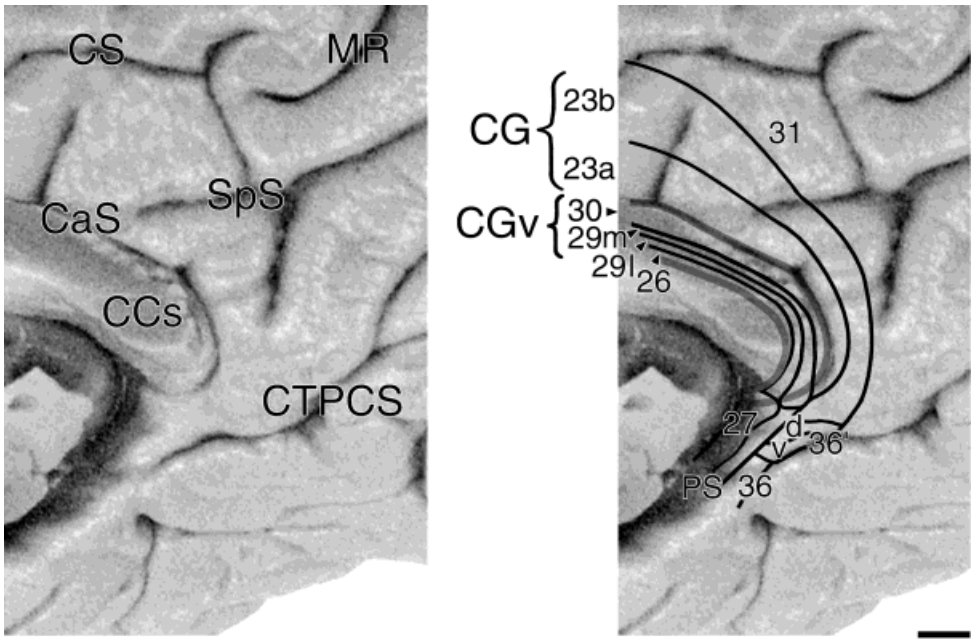

Fig. 14. The case shown in Figure 2 does not have an overt CML, but rather, the isthmus is continuous without apparent interruption and there is no gross morphologic feature associated with the transitional posterior parahippocampal area 36′. A subregional flat map was made, and the reconstruction was warped onto a photograph of this region of the brain. It was done in such a way that the splenium was reduced to show areas on the CGv. This strategy meant that areas on the cingulate gyral surface did not require reductions in the flat map. Notice how close the caudal parahippocampal areas are to the ventral edge of the splenium. Consider sections F and G in Figure 2 as evidence that the posterior cingulate and retrosplenial areas do not completely surround the splenium as shown in Brodmann's map (Fig. 1). For abbreviations, see list. Scale bar = 1 cm.

the same as for the previous case, the map was projected directly onto the brain surface, because there were so few identifying features in the CMR. The map was warped with the computer software to place it onto the photograph in such a way that areas on the CGv were placed over the splenium to avoid artificially displacing adjacent area 23. The border between areas 23a and 30, representing the ventral apex of the cingulate gyrus, is thickened in Figure 14 along the dorsal edge of the splenium. It can be seen that RSC is almost entirely located within the CaS except for a small terminal extension of area 29m that is exposed at the junction between RSC and the parahippocampal areas. As noted in the discussion of individual sections, the parahippocampal areas extend to a point just below the splenium and the RSC extends much further dorsally than suggested by Brodmann.

DISCUSSION

Review of the Brodmann (1909) map of posterior cingulate and retrosplenial cortices on the convoluted surface of the human brain in the context of immunohistochemical observations as well as those of von Economo and Koskinas (1925) suggests the need for several modifications: (1) areas 29 and 30 extend further rostral, (2) area 30 does not significantly extend onto the CML, and when area 29m does, it is to a minor extent, and (3) RSC does not extend as far ventral around the splenium. It seems that Brodmann used narrow strips of symbols, as he did for area 3 on the postcentral gyrus, to indicate that each retrosplenial area is located in CaS and the reconstruction technique required that he reduce area 23 on the CML to accommodate this representation.

The distribution of RSC and areas 23a and 23b dorsal and caudal to the splenium of the corpus callosum have been provided in complete maps of monkey and human brains based on analyses of coronal series through the entire cingulate gyrus (Vogt et al., 1987, 1995, 1997; Vogt, 1993) and the present findings substantiate these findings with immunohistochemical preparations in multiple planes of section. Furthermore, development of the retrosplenial areas has been elegantly shown with immunohistochemical analyses of coronal sections in the monkey (Berger et al., 1997). This study showed that, in the CaS, there is an arch of neurotensinergic neurons in the deep layer of areas 29 and 30, and the elaboration of these areas and their apposition to parahippocampal areas 27 and the parasubiculum was demonstrated. Morris et al. (2000) expressed concern that coronal sections through the CMR in both monkey and human "do not appropriately reveal the cellular organization of this cortical region." Although horizontal, oblique sections are useful for RSC in the CaS caudal to the splenium, this plane of section does not add to analysis of cortex on the gyral surface of the CMR. As shown in Figures 2, 3, and 6, the architecture of areas 26, 29, 30, 23a, and 23b is clear in coronal sections through the CMR. Indeed, if immunohistochemical techniques are used, the cytoarchitecture is apparent at low magnification. For example, layer IV in areas 23a and 23b on the CML is apparent in both NeuN and SMI32 preparations in human (Fig. 3) as well as neurotensin and parvalbumin immunoreactive neurons in the monkey (Berger et al.,

1997). More critical than the planes of section are the precise criteria used to identify each area.

Junction of RSC, PCC, and parahippocampal areas

An issue of general concern when localizing cortical functions in the human brain is the border between the retrosplenial/cingulate and parahippocampal cortices. Brodmann (1909) depicted RSC as fully surrounding the posterior and ventral edge of the splenium of the corpus callosum, whereas von Economo (1929) showed a termination of retrosplenial areas LE and LD at a plane caudal but not ventral to the splenium. Morris et al. (2000) show RSC more than 0.5 cm below the ventral border of the splenium and refer to a thick contingent of fibers in RSC at this ventral position. Because these fibers could be exposed by neurodegeneration like that shown in the subiculum of this case, this border may not actually extend this far ventrally. The flat maps for two cases presented in the present study show that the border between retrosplenial/posterior cingulate and parahippocampal cortices is caudal but not ventral to the splenium. Thus, the present findings fit most closely with those of von Economo (1929).

The present study sought to identify the retrosplenial extension into the calcarine sulcus previously shown in adult monkey (Vogt et al., 1987) and its developmental predecessors (Berger et al., 1997) where area 29m abuts the presubiculum and parasubiculum. A calcarine extension of area 29m could not be found in the human brain. Indeed, the monkey parieto-occipital and calcarine sulci never join to form a common trunk as in human brain, and there is not a simple redundancy in the distribution of areas in these two species in the retrocalcarine region. Instead, the rostral part of the common trunk contains a dorsal division of Braak's area properistriata (1977), and a further assessment of this issue is needed to consider the detailed structure of the dorsal bank of this sulcus.

Because the subiculum projects to RSC in monkey (Rosene and Van Hoesen, 1977), cases with significant neurodegeneration in the human subiculum might have an altered RSC architecture depending on the time and etiology of cell death. Morris et al. (2000) illustrated a case with severe neurodegeneration in the subiculum (their Fig. 2C–F). The asterisk in their Figure 1B overlies a parahippocampal region that they refer to as posteroventral retrosplenial cortex. Because the subiculum has never been reported this highly differentiated dorsal to the splenium (their Fig. 2B), it is possible that taking multiple and different planes of section around the splenium in the same hemisphere produced difficulties interpreting the levels of each section. It is also possible that defining the border between RSC and posterior parahippocampal areas is impaired in cases with substantial cell death in the subiculum, and it seems that the most ventral section in their Figure 2 did not reach the level of the asterisk shown in Figure 1B. Finally, it is necessary to provide a detailed analysis of the adjoining parahippocampal areas to ensure that differentiation of the retrosplenial areas is complete. Thus, most evidence suggests that the border between retrosplenial and posterior parahippocampal cortices occurs caudal to the ventral border of the splenium rather than around the splenium as proposed by Brodmann (1909) or substantially ventral to it as suggested by Morris et al. (2000).

The dysgranular concept

At each point of transition from allocortex to isocortex throughout the primate telencephalon, there is at least one area that has the features of a dysgranular cortex. This finding is true for orbitofrontal cortex and the insula. In the insula, neurons in layer IV are said to form islands as is characteristic of a layer that is of irregular thickness (Mufson et al., 1997). In orbitofrontal cortex, the intermediate area has a thin layer IV, which can be difficult to detect where the layer III and V pyramids are particularly large (Hof et al., 1995). Because cortex on the CGv progresses through several transitions beginning with the allocortical indusium griseum and culminating in the isocortical area 23a, the presence of a dysgranular cortex in this region needs to be considered.

Brodmann (1909) referred to area 30 as agranular and von Economo (1929) was quite explicit that his area LD is not just agranular but that the "granulous" layer of area LE (Brodmann's area 29) is not continuous with the isocortical layer of area LC2 (Brodmann's area 23). Morris et al. (2000) also state that layer III(IV) vanishes completely next to area 23. Although there is no doubt that layer III/IV in area 29 is not equivalent to layer IV in area 23a, the following three points need to be considered. First, von Economo (1929; his Fig. 50) vacillated on the presence of a layer IV in LD and showed a layer III(IV) below layer III therein. Second, our Figure 8 shows that the granular layer IV of area 29m is continuous with layer IV in area 30 and layer IV in area 23a. This does not mean that layer IV in each area is equivalent; however, von Economo's statement that they are not continuous and Morris and colleagues statement that it vanishes are not supported, because immunohistochemical preparations clearly show this continuity. Finally, the dysgranular concept for a cortical architecture was not established during the early years of cytoarchitectonic analysis nor were immunohistochemical techniques available to clarify the concept. Therefore, it is not surprising that the dysgranular structure of area 30/LD was not appreciated by early neuroanatomists.

We described the dysgranular nature of area 30 in monkey and human brains with Nissl, Golgi, and immunohistochemical techniques (Vogt, 1976; Vogt et al., 1995, 1997). Layer IV is of variable thickness with points at which layers IIIc and Va join by means of neuronal bridges across layer IV, and the present study demonstrated the dysgranular structure of layer IV in RSC by using photomontages along its full lateromedial extent in area 30. Another example of a dysgranular cortex is in anterior cingulate cortex where area 32, which sits at the juncture of anterior cingulate and prefrontal cortices, and has islands of neurons in layer IV (Vogt et al., 1995). Morris et al. (2000) took a different approach to the variable nature of layer IV of area 30 by attempting to identify agranular and dysgranular parts. However, the borders of these two parts of area 30 were not identified in the survey series of histologic preparations. In view that the goal of cytoarchitectonic studies is to identify areas with a single structure, it is difficult to understand how two fundamentally different forms of cortical organization can be subsumed by a single area.

To further document the concept of a dysgranular area 30, the present study provides different levels of magnification in two different immunohistochemical prepara-

tions. In Figure 7, the dysgranular nature of area 30 in the CaS is compared with the granular organization of area 23a on the CML. It shows the interruption of layer IV by a bridge of neurons spanning between layers IIIc and Va. However, it is difficult in single strips of cortex to fully appreciate a structure as variable as a dysgranular layer IV. Therefore, Figure 8 shows all of layer IV at a relatively high magnification in both NeuN and SMI32 preparations. The NFP-ir neuronal plexuses in layers III and V show by means of a negative image for layer IV that layer IV is continuous throughout area 30. Because most of the layer IV neurons are not immunoreactive and there are no glial or vascular elements stained, this preparation emphasizes the continuity of layer IV. The NeuN preparation shows that there are small neurons in layer IV and that there are breaks in layer IV by medium and large pyramidal neurons. The bridges of large pyramids between layers IIIc and Va are noted with asterisks. The profound differences between the architectures of dysgranular area 30 and granular area 23a are also clear in Figure 8. Thus, the dysgranular characteristics of area 30 are similar to those described previously for dysgranular areas in orbitofrontal, insular, and cingulofrontal transition areas (Hof et al., 1995; Mufson et al., 1997; Vogt et al., 1995).

Layer III of area 29m

It may seem arbitrary to term the first neuronal layer adjacent to layer I in area 29m as layer III rather than layer II. However, this selection is not the simple result of pia to white matter counting. It is based on the facts of neuron structure and the principles of cortical transition in the posterior cingulate region. It has been suggested that this is not layer II in the monkey, because these are not lancet-shaped neurons similar to those of layer II in area 23a and a distinct layer II appears only in the medial part of area 30 (Vogt, 1976).

The present study in human confirms and extends observations in monkey RSC in the following ways. First, most neurons in layer III of area 29m are NFP-ir, whereas almost none are in layer II of area 23a and medial area 30. Second, there is a reduction in the overall density of neurons and the NFP-ir dendritic plexus in the lateral part of area 30, which is adjacent to area 29m (Figs. 4, 5B). Third, the size and density of heavily NFP-ir neurons in layer III of area 29m contrasts with those in layer IIIc of area 30 (Fig. 8). It might then be concluded that neurons in layer III are most likely associated with layer IIIab as proposed previously for the monkey (Vogt, 1976). Thus, the cytoarchitecture of monkey and human cortices, Golgi studies in monkey and immunohistochemical studies in human all point to the fact that layer III of area 29 is similar to layer IIIab in neocortex rather than layers II, IIIc, or IV.

Standardized brain atlases

Because the architecture of each cortical area cannot be determined with current imaging modalities, it is imperative that standardized atlases seeking to localize Brodmann's areas rely heavily on recent neuroanatomic observations rather than Brodmann's reconstructions onto the convoluted human brain surface. The widely used Talairach and Tournoux (1988) atlas emphasized the shortcomings of Brodmann's reconstruction technique by not distinguishing areas on the gyral surfaces from those in the sulcal depths, miscalculating the depth of the CaS and areas therein, and placing areas 29 and 30 entirely on the gyral surface. Each of these difficult topologic problems can be resolved with subregional maps as first used by von Economo (1929).

Hypotheses for the present study were related to the Talairach and Tournoux (1988) interpretations of Brodmann's reconstruction, and these hypotheses could not be validated with clearly defined cytologic criteria. Thus, the presentation in this atlas needs to be considered in detail. The full depth of the CaS was accurately reconstructed in only one transverse section (Talairach and Tournoux, 1988, their Fig. 88) where it appears to have a depth of approximately 7 mm. In the next rostral section, the CaS only measures 4 mm in depth. In general, the CaS has an average depth of approximately 0.8–1 cm, and we have never observed a control case with no CaS as shown in most coronal sections in this atlas. Even cases of late-stage Alzheimer's disease with degeneration of almost all neurons have a clearly defined CaS (personal observations of the current authors). At first this may seem to be a minor point, however, if the CaS is not identified, the retrosplenial areas must be applied to the surface of the posterior cingulate cortex and CML rather than where they are actually located on the CGv. Talairach and Tournoux (1988) placed areas 29 and 30 on the posterior cingulate gyral surface, and area 30 was extended onto the posterior parahippocampal gyrus (their Figs. 87, 88) without histologic guidance. Indeed, their area 30 is located in the depths of the parieto-occipital sulcus in the parasagittal sections (their Figs. 43–46) where area 23 is shown on the medial surface reconstruction (their Fig. 9). Finally, the retrosplenial area 30 was also placed on coronal sections of the parahippocampal gyrus (their Figs. 87, 88). The flat maps of posterior cingulate and retrosplenial cortices provided by the present study should help to correctly located each of these areas on the CGv and CML/CMR for future functional imaging studies. As the structural resolution of functional imaging techniques improves, histologic guidance by higher resolution anatomic studies will be imperative.

Functions of RSC and PCC and supporting structural circuits

The boundaries of retrosplenial areas 29 and 30 and posterior cingulate areas 23 and 31 have been determined with detailed cytologic criteria and plotted in subregional flat maps for cases with different surface morphologies. Knowing the distribution of these two fundamentally different types of cortex is paramount to defining their function in imaging studies. The consequences of mislocating areas 29 and 30 are apparent in a meta-analysis that sought to determine the role of RSC in emotion (Maddock, 1999). Because this study incorrectly designated retrosplenial area 30 on the CML and added RSC activation sites to those in area 23, it was not possible to make valid statements about the specific functions of RSC. Although the role of RSC in emotion is unresolved and the problems raised in this latter study have been considered (Vogt et al., 2000), the involvement of RSC and PCC in working and visuospatial memory is not disputed. Furthermore, as the resolution of functional imaging methodologies improves, it will become possible to uncover the unique contributions of RSC and PCC to human brain function, including their role in different types of memory.

Valenstein et al. (1987) presented a case with extensive anterograde and retrograde amnesia after removal of an

arteriovenous malformation near the splenium and referred to the syndrome as retrosplenial amnesia. Involvement of the fornix may have contributed to the presentation in this case, and Parker and Gaffan (1997) placed massive cingulate cortical or anterior thalamic lesions in monkeys and tested for object-in-place memory. Interestingly, although the cingulate lesions failed to show a significant deficit in the task, there was substantial impairment in the anterior thalamic group. Because the anterior thalamic nuclei have as their primary projection the RSC (Vogt et al., 1987), it is surprising that no deficit was observed after cortical lesions. Explanations for the negative finding in the monkey are that the cortical lesions of RSC were incomplete due to the effort to remove the entire gyrus in anterior and posterior cortices and/or the task was not sensitive enough to detect a cortical impairment. There are other lines of evidence linking these two cingulate gyral areas to memory and visuospatial functions.

Working memory tasks elevate glucose metabolism in the anterior thalamic nuclei (Friedman et al., 1990). Furthermore, one of the highest levels of basal glucose metabolism in the monkey brain is in RSC and glucose metabolism in RSC is elevated when performing a delayed-response task (Matsunami et al., 1989). We have directly compared the distribution of anterior thalamic inputs with RSC and basal glucose metabolism in the monkey, and there is a striking correlation between the two (Vogt et al., 1997). The tight link between anterior thalamic projections to RSC, high levels of basal glucose metabolism, and its modulation in both structures suggest that the anterior thalamic/RSC system is a pivotal player in memory functions.

Grasby et al. (1993) activated RSC and PCC in an auditory-verbal memory task. One of the more interesting aspects of this study is that it coactivated perigenual anterior cingulate cortex in the same task. In other words, there was a large expanse of midcingulate cortex that was not activated. In view of the likely role of anterior thalamic, RSC, and PCC in memory and the joint activation of perigenual anterior cingulate cortex in some tasks, the direct and indirect connections among these areas is of new importance. Area TA is involved in auditory functions and projects directly the RSC and the CML (Van Hoesen et al., 1993; Yukie, 1995) and perigenual anterior cingulate cortex also has direct auditory afferents from the superior temporal gyrus (Vogt and Barbas, 1988). One important explanation for the joint activation of perigenual and perisplenial cingulate cortices in the auditory-verbal memory task (Grasby et al., 1993) is the shared auditory input. The relationships between perigenual and perisplenial cortices, however, are even more profound. Area 23a and RSC are reciprocally connected (Vogt et al., 1987), and the perigenual and perisplenial cortices are reciprocally connected without involvement of midcingulate cortex (Pandya et al., 1981; Vogt et al., 1987; Van Hoesen et al., 1993). Amazingly, a limbic convergence zone in area 11m receives major inputs from both perigenual and perisplenial cortices (Carmichael and Price, 1995) and pericallosal cortex in both regions receives direct subicular inputs (Rosene and Van Hoesen, 1977). Thus, primary sensory inputs, reciprocal intracingulate connections, and connections among limbic association areas preserves the functional integration of perigenual and perisplenial cortices to the exclusion of midcingulate cortex.

Another contribution of RSC and PCC to brain function is their role in topographic and topokinetic memory. Olson et al. (1993) suggested that PCC is involved in large visual scene assessment part of which is subserved by activity generated by the orbital position of the eye. Focal lesions that involve the right RSC impair memory of spatial positional relationships and are associated with topographic disorientation (Takahashi et al., 1997). Furthermore, mental navigation along memorized routes elevates blood flow in PCC (Berthoz, 1997; Ghaem et al., 1997; Maguire et al., 1998).

In conclusion, although there is little doubt that both RSC and PCC are involved in working memory and visuospatial functions, their specific contributions to each are still not known. Observations of the present report will ensure that higher resolution imaging studies with carefully controlled task designs can accurately identify the location of each of these cortical regions.

ACKNOWLEDGMENTS

The authors thank Dr. Bruce Quinn from Northwestern University for sharing his preparations of parietal cortex with NeuN and demonstrating their value for studying human cortical architecture. They also thank Linda Arcure and William Safrit for their assistance in preparing the illustrations.

LITERATURE CITED

Armstrong E, Zilles K, Schlaug G, Schleicher A. 1986. Comparative aspects of the primate posterior cingulate cortex. J Comp Neurol 253:539–548.

Berger B, Alvarez C, Pelaprat D. 1997. Retrosplenial/presubicular continuum in primates: a developmental approach in fetal macaques using neurotensin and parvalbumin as markers. Dev Brain Res 101:207–224.

Braak H. 1977. The pigment architecture of the human occipital lobe. Anat Embryol (Berl) 150:229–250.

Braak H. 1979. Pigment architecture of the human telencephalic cortex. IV. Regio retrosplenialis. Cell Tissue Res 204:431–440.

Braak H. 1980. Architectonics of the human telencephalic cortex. Berlin: Springer-Verlag.

Berthoz A. 1997. Parietal and hippocampal contribution to topokinetic and topographic memory. Philos Trans R Soc London B 352:1437–1448.

Brodmann K. 1909. Vergleichende Lokalisationslehre der Grosshirnrinde in ihren Prinzipien dargestellt auf Grund des Zellenbaues. Leipzig: Barth.

Carmichael ST, Price JL. 1995. Limbic connections of the orbital and medial prefrontal cortex in macaque monkeys. J Comp Neurol 363: 615–641.

Eriksson PS, Perfilieva E, Björk-Eriksson T, Alborn A-M, Nordborg C, Peterson DA, Gage FH. 1998. Neurogenesis in the adult human hippocampus. Nat Med 4:1313–1317.

Friedman HR, Janas JD, Goldman-Rakic PS. 1990. Enhancement of metabolic activity in the diencephalon of monkeys performing working memory tasks: a 2-deoxyglucose study in behaving rhesus monkeys. J Cogn Neurosci 2:18–31.

Ghaem O, Mellet E, Crivello F, Tzourio N, Mazoyer B, Bertholz A, Denis M. 1997. Mental navigation along memorized routes activates the hippocampus, precuneus and insula. Neuroreport 8:739–744.

Goldman-Rakic PS, Selemon LD, Schwartz ML. 1984. Dual pathways connecting the dorsolateral prefrontal cortex with the hippocampal formation and parahippocampal cortex in the rhesus monkey. Neuroscience 12:719–743.

Grasby PM, Frith CD, Friston KJ, Bench C, Frackowiak RSJ, Dolan RJ. 1993. Functional mapping of brain areas implicated in auditory-verbal memory function. Brain 116:1–20.

Hof PR, Mufson EJ, Morrison JH. 1995. Human orbitofrontal cortex cytoarchitecture and quantitative immunohistochemical parcellation. J Comp Neurol 359:48–68.

Maddock RJ. 1999. The retrosplenial cortex and emotion: new insights from functional neuroimaging of the human brain. Trends Neurosci 22:310–316.

Maguire EA, Frith CD, Burgess N, Donnett JG, O'Keefe J. 1998. Knowing where things are: parahippocampal involvement in encoding object locations in virtual large-scale space. J Cogn Neurosci 10:61–76.

Matsunami K, Kawashima T, Satake H. 1989. Mode of [^{14}C] 2-deoxy-D-glucose uptake into retrosplenial cortex and other memory-related structures of the monkey during a delayed response. Brain Res Bull 22:829–838.

Morris R, Paxinos G, Petrides M. 2000. Architectonic analysis of the human retrosplenial cortex. J Comp Neurol 421:14–28.

Mufson EJ, Sobreviela T, Kordower JH. 1997. Chemical neuroanatomy of the primate insula cortex: relationship to cytoarchitectonics, connectivity, function, and neurodegeneration. In: Bloom FE, Björklund A, Hökfelt T, editors. Handbook of chemical neuroanatomy, the primate nervous system, Vol. 13, part 1. Amsterdam: Elsevier. 377–454.

Mullen RJ, Buck CR, Smith AM. 1992. NeuN, a neuronal specific nuclear protein in vertebrates. Development 116:201–211.

Nimchinsky EA, Vogt BA, Morrison JH, Hof PR. 1997. Neurofilament and calcium-binding proteins in the human cingulate cortex. J Comp Neurol 384:597–620.

Olson CR, Musil SY, Goldberg ME. 1993. Posterior cingulate cortex and visuospatial cognition: properties of single neurons in the behaving monkey. In: Vogt BA, Gabriel M, editors. Neurobiology of cingulate cortex and limbic thalamus. Boston: Birkhäuser. p 366–380.

Pandya DN, Van Hoesen GW, Mesulam M-M. 1981. Efferent connections of the cingulate gyrus in the rhesus monkey. Exp Brain Res 42:319–330.

Parker A, Gaffan D. 1997. The effect of anterior thalamic and cingulate cortex lesions on object-in-place memory in monkeys. Neuropsychologia 35:1093–1102.

Rose M. 1928. Gyrus limbicus anterior and Regio retrosplenialis (Cortex holoprotoptychos quinquestratificatus). Vergleichende Architektonik bei Tier und Mensch. J Psychol Neurol 35:65–173.

Rosene DL, Van Hoesen GW. 1977. Hippocampal efferents reach widespread areas of cerebral cortex and amygdala in the rhesus monkey. Science 198:315–317.

Sanides F. 1970. Functional architecture of motor and sensory cortices in primates in the light of a new concept of neocortex evolution. In: Noback CR, Monagna W, editors. The primate brain. New York: Appleton Century Crofts. p 137–208.

Sarnat HB, Nochlin D, Born DE. 1998. Neuronal nuclear antigen (NeuN): a marker of neuronal maturation in the early human fetal nervous system. Brain Dev 20:88–94.

Takahashi N, Kawamura M, Shiota J, Kasahata N, Hirayama K. 1997. Pure topographic disorientation due to right retrosplenial lesion. Neurology 49:464–469.

Talairach J, Tournoux P. 1988. Co-planar stereotaxic atlas of the human brain. New York: Thieme Medical Publishers.

Valenstein E, Bowers D, Verfaellie M, Heilman KM, Day A, Watson RT. 1987. Retrosplenial amnesia. Brain 110:1631–1646.

Van Hoesen GW, Morecraft RJ, Vogt BA. 1993. Connections of the monkey cingulate cortex. In: Vogt BA, Gabriel M, editors. Neurobiology of cingulate cortex and limbic thalamus. Boston: Birkhäuser, p 249–284.

Vogt BA. 1976. Retrosplenial cortex in the rhesus monkey: a cytoarchitectonic and Golgi study. J Comp Neurol 169:63–98.

Vogt BA. 1993. Structural organization of cingulate cortex: areas, neurons, and somatodendritic transmitter receptors. In: Vogt BA, Gabriel M, editors. Neurobiology of cingulate cortex and limbic thalamus. Boston: Birkhäuser. p 14–70.

Vogt BA, Barbas H. 1988. Structure and connections of the cingulate vocalization region in the rhesus monkey. In: Newman JD, editor. The physiological control of mammalian vocalization. NY: Plenum. p 203–225.

Vogt BA, Pandya DN, Rosene DL. 1987. Cingulate cortex of the rhesus monkey. I. Cytoarchitecture and thalamic afferents. J Comp Neurol 262:256–270.

Vogt BA, Nimchinsky EA, Vogt LJ, Hof PR. 1995. Human cingulate cortex: surface features, flat maps, and cytoarchitecture. J Comp Neurol 359: 490–506.

Vogt BA, Vogt LJ, Nimchinsky EA, Hof PR. 1997. Primate cingulate cortex chemoarchitecture and its disruption in Alzheimer's disease. In: Bloom FE, Björklund A, Hökfelt T, editors. Handbook of chemical neuroanatomy, the primate nervous system, Vol. 13, part 1. Amsterdam: Elsevier. p 455–528.

Vogt BA, Absher JR, Bush G. 2000. Human retrosplenial cortex: where is it and is it involved in emotion? Trends Neurosci 23:195–196.

von Economo C. 1929. The cytoarchitectonics of the human cerebral cortex. London: Oxford University Press.

von Economo C, Koskinas GN. 1925. Die Cytoarchitektonik der Hirnrinde des erwachsenen Menschen. Berlin: Springer.

Wolf HK, Buslei R, Schmidt-Kastner R, Schmidt-Kastner PK, Pietsch T, Wiestler OD, Blumcke I. 1996. NeuN: A useful neuronal marker for diagnostic histopathology. J Histochem Cytochem 44:1167–1171.

Yukie M. 1995. Neural connections of auditory association cortex with the posterior cingulate cortex in the monkey. Neurosci Res 22:179–187.

Zilles K. 1990. Cortex. In: Paxinos G, editor. The human nervous system. San Diego: Academic Press. p 757–802.